Section 2

Data sets, diagnostic and dynamical investigations, statistical post-processing , multi-year reanalyses and associated studies

About Warming in Troposphere over North-West of Russia

Oleg A. Alduchov and Irina V. Chernykh

Russian Institute of Hydrometeorological Information – Word Data Center, Obninsk, Russia,
E-mail: aoa@meteo.ru, civ@meteo.ru

At present time the study of climate change in Arctic region, in particular Russian part of Arctic, is very actual by reason of sensible warming in the region and absence of clear understanding of the reason of the warming. The research of climatic changes of temperature at the standard isobaric levels in Arctic troposphere over period 1964-10.2007 years is presented on base of radiosonde sounding data from dataset CARDS [Eskridge et al, 1995] for two stations: Murmansk and Nar'jan-Mar, placed in North-West of Russia. The method based on the using of hourly observations with taking into account the possible time correlations of observations [Alduchov and Chernykh, 2008] was used for calculating linear trends in time series of temperature anomalies at the standard isobaric levels. The method was developed especially for estimate of trends for Polar Regions with probably not full time series of observations. It is shown that warming for year with significance not less than 95% was detected over Murmansk only in low troposphere and over Nar'jan-Mar at most levels of troposphere. The largest warming for both stations was detected at level 925 hPa for January with decadal changes 0.71ºC/dec. and 0.95ºC/dec. for Murmansk and Nar'jan-Mar correspondently.

It is known, the estimations of trends are partly dependent from homogeneity and quality data. Note, that number of observations for 00 and 12 GMT is practically the same for both stations. Numbers of observations before and after running of complex quality control procedure [Alduchov and Eskridge, 1996] are presented in tables 1 and 2 for different months, seasons and year for level 850 hPa. Number of rejected observations foot up to 0.7% (Murmansk) and 0.9% (Nar'jan-Mar) from all soundings (table 2).

TABLE 1. Number of T observations before and after complex quality control for level 850 hPa for different months.

Station	Jan.	Feb.	Mar.	Apr.	May	Jun.	Jul.	Aug.	Sep.	Oct.	Nov.	Dec.
Murmansk	2552	2329	2526	2468	2574	2356	2283	2343	2431	2459	2404	2509
	2543	2309	2500	2456	2563	2341	2242	2324	2413	2442	2396	2496
Nar'jan-Mar	2393	2224	2426	2381	2356	2359	2424	2344	2204	2304	2169	2328
	2382	2205	2398	2354	2329	2337	2395	2318	2189	2285	2149	2313

TABLE 2. The same as TABLE 1 for seasons and for year.

Station		Winter	Spring	Summer	Autumn	Year	Year (%)
Murmansk	Before control	7390	7568	6982	7294	29234	100
	After control	7348	7519	6909	7251	29027	99.3
Nar'jan-Mar	Before control	6945	7163	7127	6677	27912	100
	After control	6900	7081	7050	6623	27654	99.1

The multiannual means of temperature are presented for different months, seasons and for year at figure 1a. Corresponding linear trends in time series of temperature anomalies at the standard isobaric levels in troposphere are presented at figure 1b-1d. Due continuity of climatic changes in atmosphere all detected trends (with different significance), trends with significance not less than 50% and trends with significance not less than 95% are presented at the figure 1b-1d.

Figure 1b demonstrates the inhomogeneous of climatic changes in Arctic troposphere. Warming is detected only in low troposphere over Murmansk for all months, seasons and year in total. Only for autumn's months and autumn in total the warming is detected in middle and high troposphere too. Small cooling was detected in middle and/or high levels of troposphere for other months and for year in total. Warming over Nar'jan-Mar is detected for all months (with exception February, August and December), seasons (with exception winter) and year at all levels in troposphere. Cooling is detected in middle troposphere over Nar'jan-Mar for February and for winter, in low troposphere - for August and at all levels - for December. Figure 1c shows that not all determined trends were detected with significance more than 50% for both stations.

The warming with significance not less than 95% was detected over Murmansk only for January, April, spring, autumn and year only in low troposphere and over Nar'jan-Mar - only for June and autumn in middle and high troposphere, for spring – in low troposphere and for year - at most levels of troposphere (Fig. 1d).

Linear trends values for temperature anomalies for levels 925 hPa, 850 hPa and 700 hPa are presented in Table 3 for January, spring, autumn and year. Table 3 shows the largest warming for both stations was detected at level 925 hPa for January. For Murmansk it was detected with decadal changes 0.71ºC/Dec. and for Nar'jan-Mar it was detected with decadal changes 0.95ºC/Dec. For year largest warming was detected at level 925 hPa for Murmansk and for Nar'jan-Mar with decadal changes 0.42ºC/Dec. and 0.38 ºC/Dec. correspondently.

The results can be used for modeling of climate change, in study of climate change in Arctic region.

Acknowledgment. Study was supported by RBRF, project 07-05-00264.

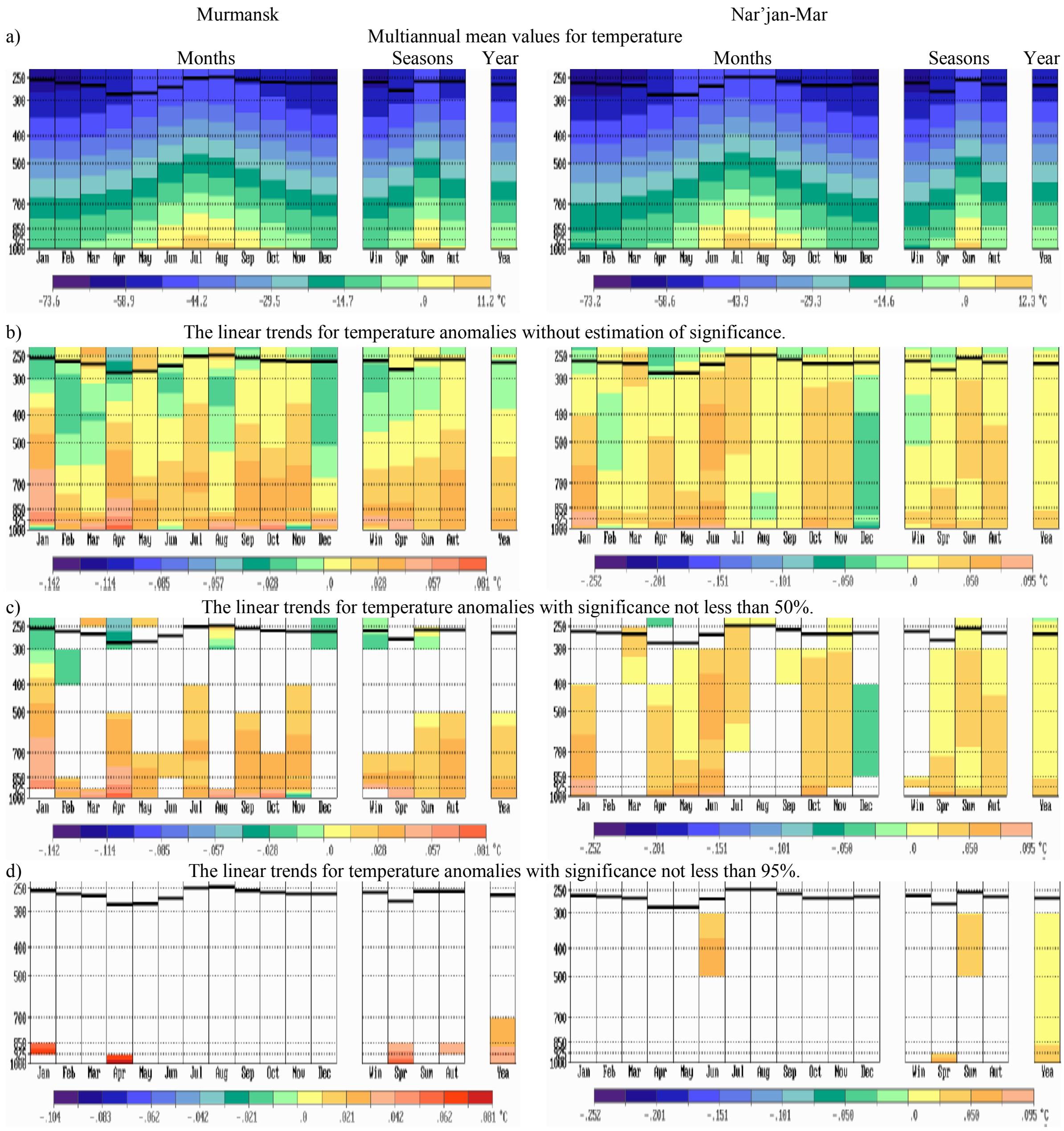

Fig. 1. Multiannual mean values for temperature (a) and linear trends for temperature anomalies (ºC/year) for the isobaric levels calculated on the base of hourly observations with taking into account the time correlations of observations for different months (in the left), seasons (in the center) and for year (in the right) without estimation of significance (b), with significance not less than 50% (c) and 95% (d). The first tropopause is marked by black line. Stations: Murmansk (left column) and Nar'jan-Mar (right column). CARDS. 1964 – 10.2007.

TABLE 3. Linear trends for temperature anomalies (ºC/decade) for standard isobaric levels 925 hPa, 850 hPa and 700 hPa, calculated on the base of hourly observations with taking into account the time correlations of observations, for January, spring, autumn and year. Trends with significance 99% are marked by Italic. Significance of other trend is not less than 85%.

Station	January			Spring			Autumn			Year		
	Standard isobaric levels, hPa											
	700	850	925	700	850	925	700	850	925	700	850	925
Murmansk	.50	.53	*.71*	.20	.32	.45	.34	.32	-	*.24*	*.28*	*.42*
Nar'jan-Mar	.58	.67	*.95*	.24	.30	.45	.27	.31	.38	*.21*	*.23*	*.38*

REFERENCES

Alduchov O.A., Chernykh I.V. About changes of temperature-humidity regime in troposphere over Antarctic Peninsula // Proc. RIHMI-WDC. 2008, 173, 270-294.

Alduchov O.A., Eskridge R.E. Complex quality control of upper air parameters at mandatory and significant levels for the CARDS dataset // NCDC Report. 1996. 151 pp.

Eskridge R.E., Alduchov O.A., Chernykh I.V., Zhai P., Doty S.R., Polansky A.C. A Comprehensive Aerological Reference Data Set (CARDS): Rough and systematic errors // Bull. Amer. Meteor. Soc. 1995, **76**, 1959-1775.

About Increasing of Water Vapour Amount in Troposphere over North-West of Russia

Oleg A. Alduchov and Irina V. Chernykh

Russian Institute of Hydrometeorological Information – Word Data Center, Obninsk, Russia,
E-mail: aoa@meteo.ru, civ@meteo.ru

The warming in Arctic region is one of actual problems both for science and for economic. In particular warming in troposphere leads to increasing of moisture capacity of atmosphere. But water vapour is one of greenhouse gases. Moreover changes in distributions of temperature and humidity in troposphere can lead to changes of macrostructure of cloudiness. Below estimations of climatic changes for water vapour amount (VA) for standard isobaric levels in troposphere over part of Arctic region, over North-West of Russia, are presented on base dataset CARDS [Eskridge et al, 1995] over period 1964-10.2007 years for stations Murmansk and Nar'jan-Mar. The method for detecting of trends [Alduchov et al, 2006, Alduchov, Chernykh, 2008], developed especially for study of climatic changes over Polar Regions with probably not full time series of observations, was used for estimations. It is shown that water vapour amount is increasing with significance not less than 95% over Murmansk in low troposphere for autumn and year and over Nar'jan-Mar - in high troposphere for summer, autumn and year.

Time series of observations for these arctic stations are enough full. Number of sounding for 00 GMT and 12 GMT are practically the same. Number of humidity observations used for researches have shown in Table for different months for standard isobaric levels: 850 hPa, 700 hPa, 500 hPa and 400 hPa. Nevertheless Table demonstrates some inhomogeneous in humidity data by reason of the decreasing with height of number of humidity observations, especially in cold months.

TABLE. Number of humidity observations used for researches for different standard isobaric levels for different month

Level (hPa)	Month											
	1	2	3	4	5	6	7	8	9	10	11	12
	Murmansk											
400	1747	1548	1720	1752	1848	1867	1811	1890	1899	1897	1699	1702
500	2109	1908	2080	2006	2061	1894	1821	1907	1984	2084	1993	2010
700	2194	1961	2123	2068	2072	1905	1828	1917	1994	2118	2055	2115
850	2194	1964	2121	2070	2071	1908	1831	1922	1994	2123	2060	2120
	Nar'jan-Mar											
400	1473	1330	1541	1597	1708	1887	1942	1872	1689	1651	1421	1454
500	1828	1662	1932	1911	1881	1901	1951	1890	1766	1873	1726	1794
700	1963	1827	2021	1960	1896	1907	1968	1907	1770	1895	1780	1891
850	1963	1825	2019	1963	1899	1908	1971	1902	1776	1894	1779	1889

The multiannual monthly mean values for VA for isobaric levels and linear trends in correspondent time series for VA anomalies, calculated on the base of hourly observations with taking into account the time correlations of observations are presented at Figure 1. The trends are presented for different months, seasons and for year without estimation of significance, with significance not less than 50% and not less than 95%.

Figure 1a demonstrates that biggest mean values of VA in troposphere over both stations take place in summer. For 500 hPa it equal to 16.5 kg/m^2 for Murmansk and 17.4 kg/m^2 - for Nar'jan-Mar. But tendencies of climatic changes of VA for summer are some different for the stations. Most increasing of VA for summer was detected over Murmansk - in low troposphere and over Nar'jan-Mar - in high troposphere (fig. 1b, 1c). For example, trends of VA for 850 hPa, detected with significance 88% and 82%, equal to 0.11 kg/m^2/decade and 0.14 kg/m^2/decade for Murmansk and Nar'jan-Mar correspondently. Trends of VA for 300 hPa, detected for summer with significance 60% and 99%, equal to 0.13 kg/m^2/decade and 0.65 kg/m^2/decade for Murmansk and Nar'jan-Mar correspondently.

Figure 1d shows that trends with significance not less than 95% are detected only in low troposphere over Murmansk for autumn and year (for 850 hPa trends equal to 0.14 kg/m^2/decade and 0.1 kg/m^2/decade correspondently); over Nar'jan-Mar its are detected in low troposphere only for year (for 850 hPa decadal changes equal to 0.1 kg/m^2/decade), in middle troposphere - for January, autumn and year (for 400 hPa decadal changes equal to 0.35 kg/m^2/decade, 0.45 kg/m^2/decade, 0.29 kg/m^2/decade correspondently). The trends with significance not less than 95% are detected in high troposphere over Nar'jan-Mar for summer, autumn and year (for 300 hPa decadal changes equal to 0.65 kg/m^2/decade, 0.44 kg/m^2/decade, 0.32 kg/m^2/decade correspondently).

Note, warming for year with significance not less than 95% was detected only in low troposphere over Murmansk and at all levels in troposphere over Nar'jan-Mar [Alduchov, Chernykh, 2009]. Moreover, it was founded the decreasing for low boundary of cloud layers with cloud amount 80-100% of the sky for year for both stations [Chernykh, Alduchov, 2009].

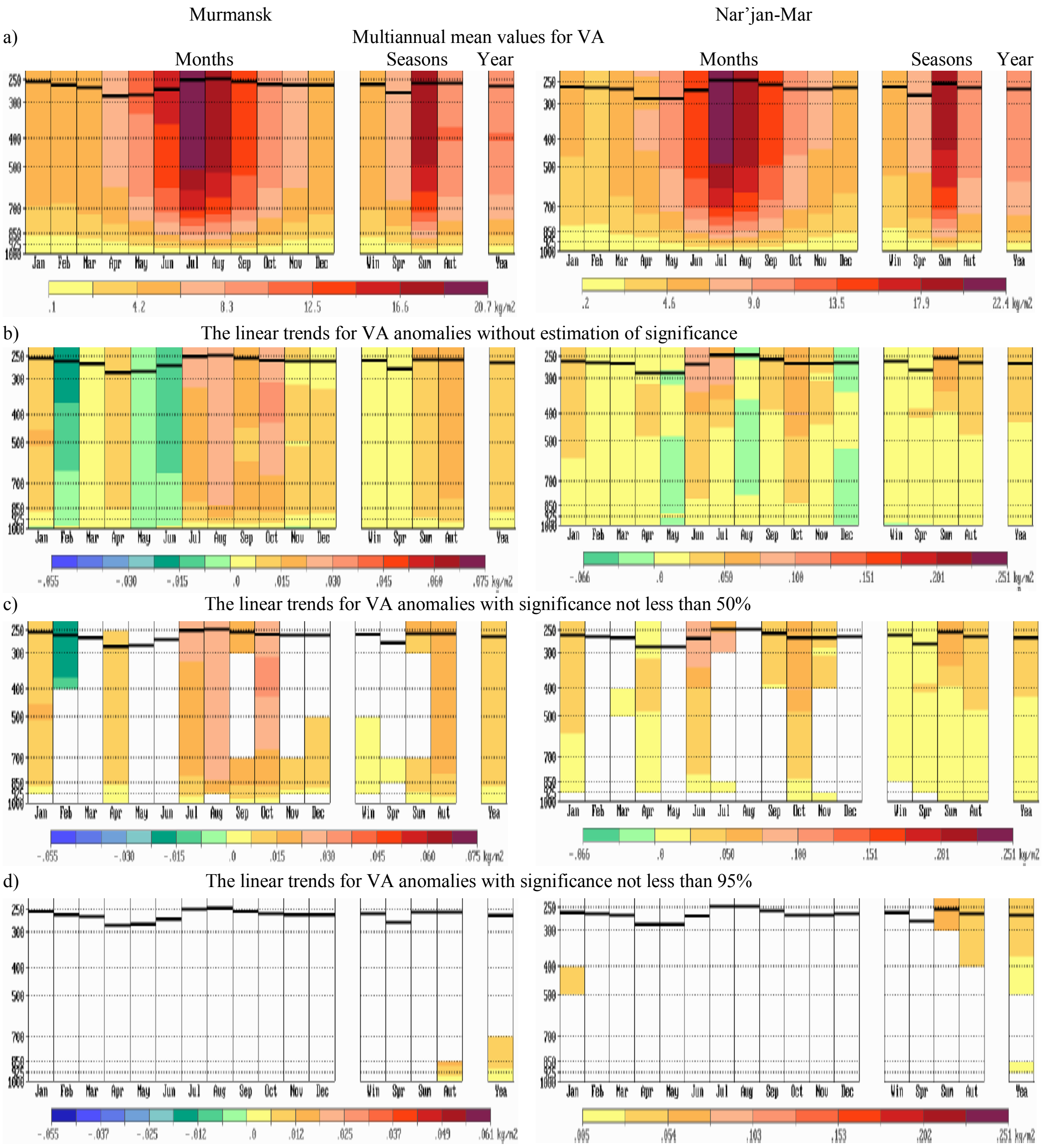

Fig. 1. Multiannual mean values (kg/m^2) for vapour amount VA (a) and linear trends in time series of vapour amount anomalies (kg/m^2/year) for the isobaric levels calculated on the base of hourly observations with taking into account the time correlations of observations for different months (in the left), seasons (in the center) and for year (in the right) without estimation of significance, with significance not less than 50% (c) and 95% (d). The first tropopause is marked by black line. Stations Murmansk (left column) and Nar'jan-Mar (right column). CARDS. 01.1964 – 10.2007.

The results can be used for analysis of climate change of humidity, cloudiness, precipitation for Arctic region.

Acknowledgment. Study was supported by Russian Basic Research Foundation (RBRF), project 07-05-00264.

References

Alduchov O.A., Chernykh I.V. About changes of temperature-humidity regime in troposphere over Antarctic Peninsula // Proc. RIHMI-WDC. 2008., 173. 270-294.

Alduchov O.A., Chernykh I.V. About warming in troposphere over North-West of Russia // Research Activities in Atmospheric and Oceanic Modelling. WMO. http://collaboration.cmc.ec.gc.ca/science/wgne/BlueBook/ 2009.

Alduchov O.A., Lagun V. E., Chernykh I.V., Jagovkina S.V. About climatic changes of troposphere over Antarctic peninsula. - "Problemy Klimatologi Polarnej". 2006. **16.** 7-22.

Chernykh I.V., Alduchov O.A. Trends in low boundary of overcast clouds over North-West of Russia// Research Activities in Atmospheric and Oceanic Modelling. WMO. http://collaboration.cmc.ec.gc.ca/science/wgne/BlueBook/ 2009.

Eskridge R.E., Alduchov O.A., Chernykh I.V., Zhai P., Doty S.R., Polansky A.C. A Comprehensive Aerological Reference Data Set (CARDS): Rough and systematic errors // Bull. Amer. Meteor. Soc. 1995. **76.** 1959-1775.

A comparison between observed and GCM simulated seasonal variations in the deuterium excess of precipitation

Nikolaus Buenning[1], David Noone[1]
[1] *Cooperative Institute of Research in Environmental Sciences and the Department of Atmospheric and Oceanic Sciences, University of Colorado, Boulder, CO, USA*
(Email: buenning@colorado.edu)

Isotopes in precipitation are widely used for both hydrology and climate variability studies. The deuterium excess in precipitation is defined as $d = \delta D - 8\delta^{18}O$ where $\delta = (R/R_{STANDARD} - 1) \times 1000$, and R is the heavy to light isotope ratio ($\delta^{18}O$ for $H_2{}^{18}O$ and δD for HDO) [*Dansgaard,* 1964]. As water undergoes phases changes under equilibrium conditions, kinetic effects arise due to the different molecular weights and different diffusion rates between HDO and $H_2{}^{18}O$. The resulting kinetic effects will cause δD and $\delta^{18}O$ values to deviate from the 8:1 ratio that results from equilibrium processes. These kinetic effects are sometimes results of vapor deposition during snow formation when the environment is supersaturated over ice and other times it is a result of raindrop evaporation and subsequent exchanges with the environmental air [*Jouzel and Merlivat*, 1984; *Stewart*, 1975]. Furthermore, it has been shown that a clear relationship exists between *d* values and source region sea surface temperatures (positively related) and the relative humidity (negatively related) [*Craig and Gordon*, 1965; *Merlivat and Jouzel*, 1979; *Johnsen et al.*, 1989]. Though many of these studies have revealed much about the correlations and physics involved with both the spatial and temporal variations in *d* values, little attention has been given to the global seasonal variation in *d* values. The work here makes use of station observations (from Global Network for Isotopes in Precipitation, GNIP) to identify areas with large seasonal variations in *d* values, and compares these with simulations of *d* from three General Circulation Models (GCMs) (MUGCM, ECHAM, and GISS) to assess if the models are simulating the proper controls on *d* values in regions where seasonal amplitudes are high. A Cressman-like objective analysis [Cressman, 1959] is used to interpolate the 12 monthly means of observed *d* values onto a grid for comparison with GCM output.

The seasonal means of *d* values (Figure 1) reveal that the largest seasonal variations are over the Southwest U.S. and the Antarctic Peninsula. It is likely that these two large variations are caused by somewhat similar processes. In the Southwest U.S., there is a shift in the winds during the summer months that bring in vapour from deep within the Gulf of California and with it higher rainfall totals. This monsoonal effect could have two effects: 1) vapour that is derived from tropical regions will have a higher source water relative humidity, and 2) the increase in rain will likely cause more precipitation re-evaporation. Both of these will lead to lower *d* values during the summer months and lead to the large observed seasonal variation. Over the Antarctica Peninsula, there is also a seasonal shift in the moisture transport paths as the Antarctic High becomes less intense during the December-February months. This large seasonal variation in *d* values could also be linked to the seasonality of sea-ice conditions and supersaturation within clouds.

The GCMs are unable to correctly simulate the magnitude of these two large seasonal variations (Figures 1c and 1d). In the Southwest U.S., the GCMs are completely unable to capture the low *d* values during the Northern Hemisphere summer months. This could be a result of improper simulations of the North American Monsoon, either from incorrect shifts in wind direction and source water regions or lack of rainfall re-evaporation during intense rainfall events. The GCMs also do not capture the large seasonal variation seen near the Antarctica Peninsula, which could be due to improper seasonal wind shifts and cloud conditions. The models do simulate a large seasonal variation over a broad region of the subtropics that encompasses Northeast Africa, the Middle East, and northern India, and likely tied to improper timing or improper strength of the monsoon.

These findings have revealed that in certain regions some components of the hydrological cycle are improperly simulated with GCMs. The regions of most concern are regions where there are large seasonal wind shifts (monsoonal regions), which is likely a consequence of the dependence of *d* values on source water regions.

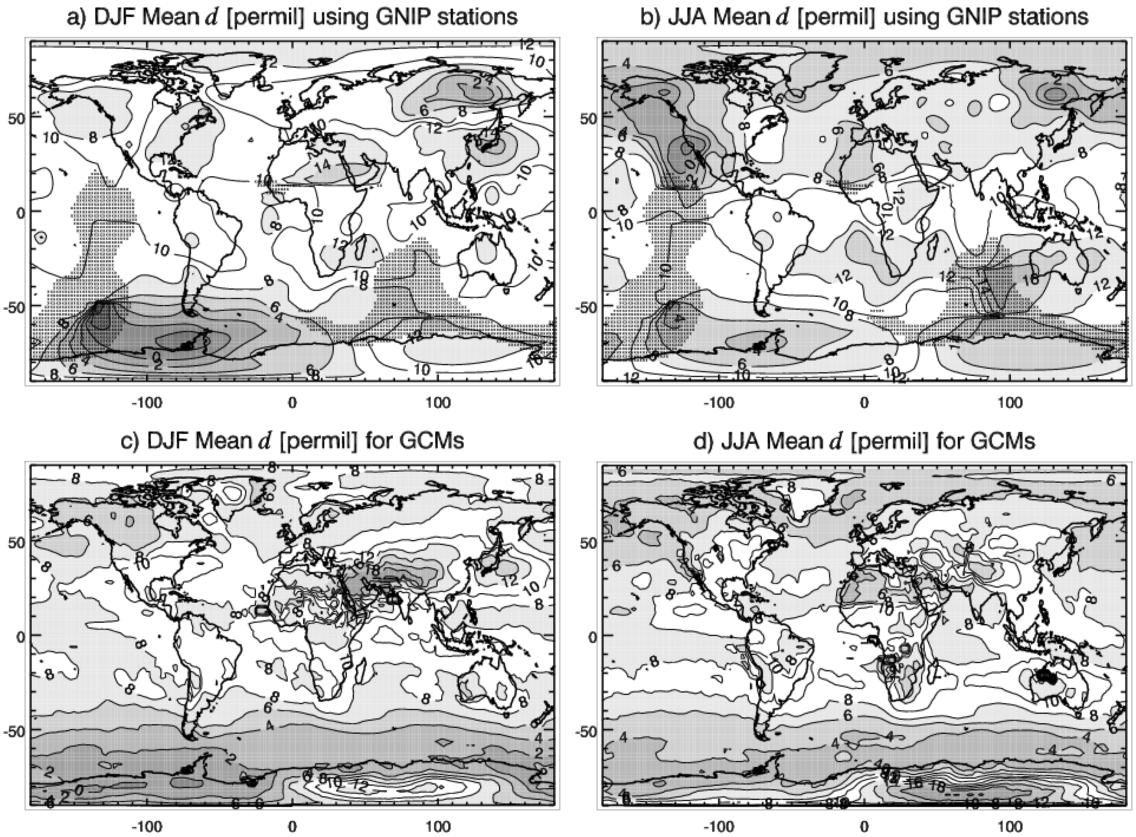

Figure 1. Seasonal means in *d* values (‰) for the (a-b) interpolated observations and (c-d) GCM mean. In a and b, stippling is added in areas with few stations.

Craig, H., and L. Gordon (1965), Deuterium and Oxygen-18 variations in the ocean and the marine atmosphere. In E. Tongiorgi (Ed.) Proceedings of a conference on *Stable isotopes in oceanic studies and paleotemperatures* Laboratory of Geology and Nuclear Sciences, Pisa, Italy, 9-30.

Cressman, G. P., An operative objective analysis system, *Mon. Weather Rev.*, **87**, 367-374, 1959.

Dansgaard, W. (1964), Stable isotopes in precipitation, *Tellus*, *16*, 436-468.

Johnsen, S. J., W. Dansgaard, and J. W. C. White (1989), The origin of Arctic precipitation under present and glacial conditions, *Tellus, Ser. B, 41*, 452-468.

Jouzel, J. and L. Merlivat (1984), Deuterium and oxygen 18 in precipitation: modeling of the isotopic effects during snow formation, *J. Geophys. Res*, *89*, 11,749-11,757.

Merlivat, L., and J. Jouzel (1979), Global climatic interpretation of the deuterium-oxygen 18 relationship for precipitation. *J. Geophys. Res.*, *84*, 5029-5033.

Stewart, M. K. (1975), Stable Isotope Fractionation Due to Evaporation and Isotopic-Exchange of Falling Waterdrops – Applications to Atmospheric Processes and Evaporation of Lakes, *J. Geophys. Res*, *80*(9), 1133-1146.

Trends in Low Boundary of Overcast Clouds over North-West of Russia

Irina V. Chernykh and Oleg A. Alduchov

Russian Institute of Hydrometeorological Information – Word Data Center, Obninsk, Russia,
E-mail: civ@meteo.ru, aoa@meteo.ru

Cloudiness is one of main components of climatic system, but its climatic changes, in particular climatic changes of low boundary of overcast clouds over Arctic region, are not fully studied. Earlier it have been shown for Globe for the period 1964-1998 years that low boundary means for cloud layers with cloud amount 80-100% of the sky (overcast clouds) in atmospheric layer 0-10 km are decreasing for central months of the seasons (January, April, July, October) separately and in total with decadal changes of -27 m/decade, -27 m/decade, -19 m/decade, -25 m/decade and -24 m/decade correspondently [Chernykh, Alduchov, 2000; Chernykh et al, 2001]. The estimations of low boundary means for cloud layers with cloud amount 80-100% of the sky (LBO) and trends in LBO are presented in this paper for part of Arctic region, North-West of Russia, more particularly: for different months, seasons and for year for different atmospheric layers. Moreover, linear trends in time series of LBO anomalies were calculated by the method based on the using of observations with taking into account the possible time correlations of observations [Alduchov et al, 2006]. The results demonstrate inhomogeneous in the changes of LBO in time and space. It is shown the decreasing of LBO and the decreasing of annual and interseasonal variability for LBO in different atmospheric layers.

CE-method for cloud amount and boundaries reconstruction [Chernykh, Alduchov, 2004] and radiosonde sounding data from CARDS [Eskridge et al, 1995] for two stations: Murmansk and Nar'jan-Mar for period 1964-2007 years were used for this research. Number of detected cloud layers with cloud amount 80-100% of the sky in different atmospheric layers for period 1964-2007 years and number of sounding presented in the Table. It demonstrates some specific in vertical macrostructure of cloudiness over the stations.

TABLE. Number of cloud layers with cloud amount 80-100% of the sky in different atmospheric layer for period 1964-2007 years and number of sounding (N)

Station	Atmospheric layer						N
	0-2 km	2-6 km	6-10 km	0-6 km	2-10 km	0-10 km	
Murmansk	12916	12319	14947	15121	16910	15681	29234
Nar'jan-Mar	13054	10331	13774	13624	15002	13651	27912

The multiannual means and trends in time series of LBO anomalies for the atmospheric layers 0-2 km, 2-6 km, 6-10 km, 0-6 km, 2-10 km, 0-10 km over surface level are presented at figure 1. Due continuity of climatic changes in time and space all detected trends (with different significance), trends with significance not less than 50% and trends with significance not less than 95% are presented at the figure 1b, 1c, 1d correspondently.

For example (fig. 1a), multiannual averages for LBO in the atmospheric layer 0-2 km are 0.57 km for Murmansk and 0.5 km - for Nar'jan-Mar. In atmospheric layer 0-10 km they are about 2.4 km for Murmansk and 2.2 km - for Nar'jan-Mar.

Figure 1b shows decreasing of LBO for year for every of the atmospheric layers for both stations. Largest decreasing of LBO for year was detected in atmospheric layers 0-10 km and 2-10 km for Murmansk with decadal changes -0.39 km*decade^{-1} and -0.23 km*decade^{-1} and for Nar'jan-Mar - with decadal changes -0.43 km*decade^{-1} and -0.38 km*decade^{-1} correspondently.

Decreasing of the LBO in atmospheric layers 0-2 km and 2-6 km for year were detected for Murmansk with decadal changes -19 m*decade^{-1} and -42 m*decade^{-1} and for Nar'jan-Mar with decadal changes -40 m*decade^{-1} and -71 m*decade^{-1}, correspondently. Decreasing of the LBO go together with warming in low troposphere [Alduchov, Chernykh, 2009a], increasing of water vapour amount in troposphere [Alduchov, Chernykh, 2009b], increasing in the frequency of cloud layers in atmospheric layer 0-2 km and 2-6 km over the stations with decadal changes in 4%*decade^{-1} and 2%*decade^{-1} over Murmansk and 6%*decade^{-1} and 4%*decade^{-1} over Nar'jan-Mar. Significance of all trends for year is not less than 99%.

Figure 1b for different months and seasons demonstrates that climatic changes of LBO in Arctic atmosphere are inhomogeneous in the time and space. Figure shows the decreasing of annual and interseasonal variability for LBO in atmospheric layer 0-10 km, 6-10 km for both stations: maximum decreasing for LBO are detected for spring and/or summer, when mean values are largest (fig. 1a). Decreasing of annual and interseasonal variability for LBO in atmospheric layer 2-6 km follows from increasing LBO in summer, when mean values are lowest, and decreasing in other seasons.

The results can be used for comparison with estimations of cloudiness changes, obtained on base surface and satellites observations, in aviation needs, in study of climate change in Arctic region.

Acknowledgment. Study was supported by RBRF, project 07-05-00264.

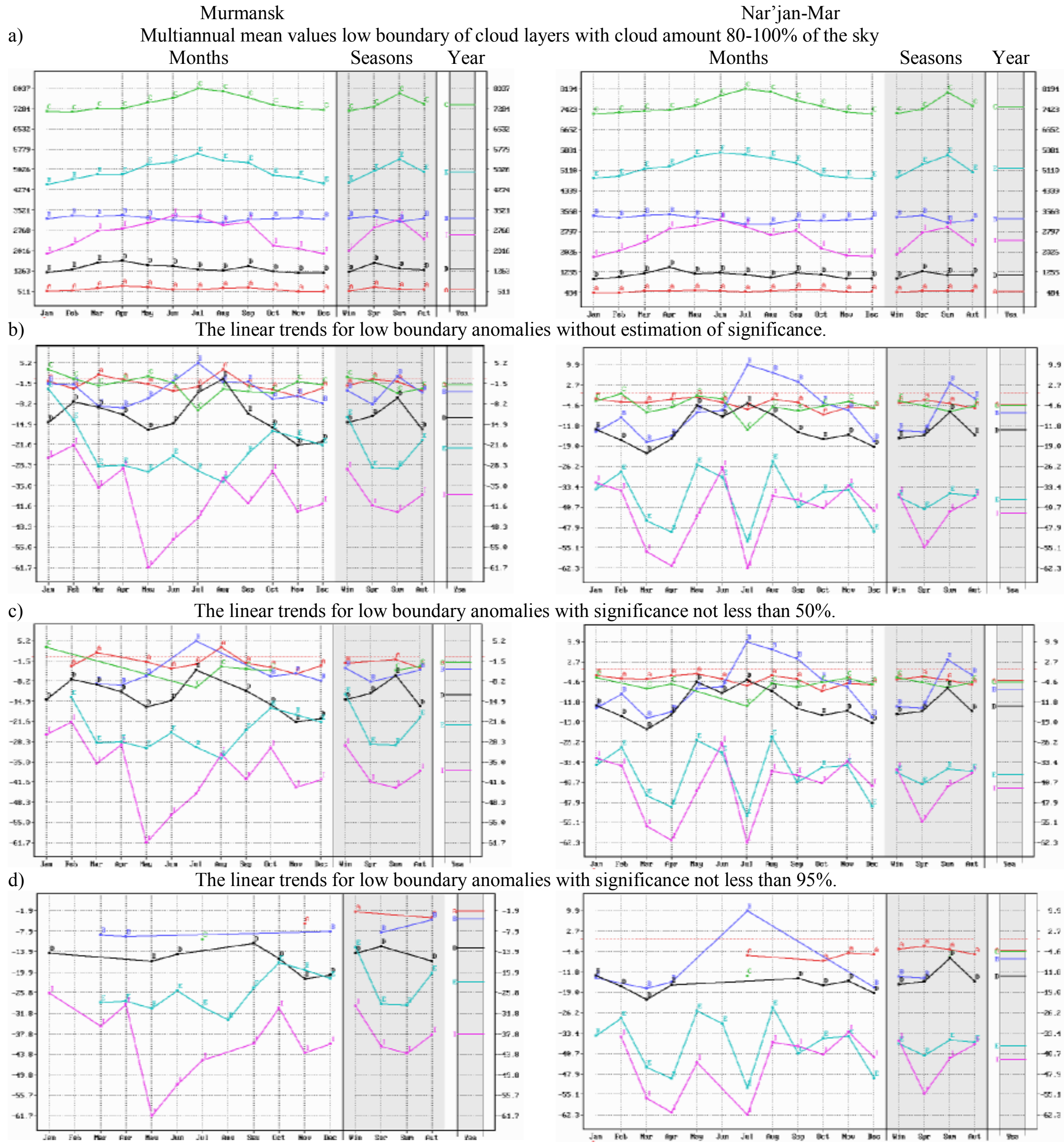

Figure 1. (a) Multiannual mean values (m) for low boundary of cloud layers with cloud amount 80-100% of the sky for different months, seasons and for year in different atmospheric layers: 0-2 km - (A, red lines), 2-6 km - (B, navy lines), 6-10 km - (C, green lines), 0-6 km – (D, black lines), 2-10 km – (E, blue lines), 0-10 km – (I, pink lines). (b) - (d) Corresponding linear trends for anomalies of low boundary (m/year), calculated on the base of hourly observations with taking into account the time correlations of observations. Stations: Murmansk and Nar'jan-Mar. CARDS. 01.1964 - 10.2007.

References

Alduchov O.A., Lagun V. E., Chernykh I.V., Jagovkina S.V. About climatic changes of troposphere over Antarctic peninsula // "Problemy Klimatologi Polarnej". 2006. **16.** 7-22.

Alduchov O.A., Chernykh I.V. About warming in troposphere over north-west of Russia // Research Activities in Atmospheric and Oceanic Modelling. WMO. http://collaboration.cmc.ec.gc.ca/science/wgne/BlueBook/ 2009a

Alduchov O.A., Chernykh I.V. About increasing of water vapour amount in troposphere over north-west of Russia // Research Activities in Atmospheric and Oceanic Modelling. WMO. http://collaboration.cmc.ec.gc.ca/science/wgne/BlueBook/ 2009b

Chernykh I.V., Alduchov O.A. Trends of some parameters of the cloudy sky reconstructed from CARDS of 1964-1998 // Proceedings of 24 Annual Climate Diagnostics and Prediction Workshop. Arizona. November 5-9, 1999. 187-190.

Chernykh I.V., Aldukhov O.A. Vertical distribution of cloud layers from cloud radiosounding data // Izvestiya, Atmospheric and Oceanic Physics. 2004. **40.** No 1. 41-53.

Chernykh I.V., Alduchov O.A., Eskridge R. E. Trends in low and high cloud boundaries and errors in height determination of cloud boundaries // Bull. of Amer. Met. Society. 2001. **82.** 1941–1947.

Eskridge R.E., Alduchov O.A., Chernykh I.V., Zhai P., Polansky A.C., Doty S.R. A comprehensive aerological reference dataset (CARDS): rough and systematic errors // Bull. Amer. Meteor. Soc. 1995. **76.** 1759-1775.

The objective analysis of three-dimensional geometry of atmospheric fronts

V. A. Gordin, Hydrometeocentre of Russia, Higher School of Economics, E-mail: vagordin@mail.ru

Ph. L. Bykov, Hydrometeocentre of Russia, Higher School of Economics, Moscow State University, E-mail: bphilipp@inbox.ru

We try to evaluate atmospheric fronts' geometry on standard baric levels according to data of the objective analysis (or of the forecast) on the global regular latitude–longitudinal grid. The algorithm of such evaluation is offered.

Then we evaluate correlation functions (CF) for the principal meteorological fields as functions of a distance between pairs of points. We consider two pairs' ensembles: i) these two points are separated by a frontal line; ii) both points are not separated by any frontal line.

The difference between these CF is significant, that confirms our algorithm's quality.

1. New predictors of the frontal zones were used. Maximal eigen-values of the following matrices: Jacobi matrix of the horizontal wind and Hesse matrix of the geopotential or pressure on the sea level separate frontal zones better than traditional predictors: vertical component of wind's vorticity and Laplacian of the geopotential or pressure on the sea level, respectively. All the predictors are suitable for ideal media models, because they are equal to infinity on tangential discontinuity. However, for real viscous media (were the values are large but limited) new predictors are preferable.

2. To calculate first and second derivatives for the new predictors on a regular discrete two-dimensional grid we use fast Fourier transformation in the spherical case or 4–th order compact schemes in the plane one. The methods are more exact than traditional 2–th order's approaches. Then we "mix" the new predictors.

3. Heuristic methods of thin frontal zones evaluation along "crests" predictor were developed.

4. When the frontal lines are constructed, we evaluate two kinds of CF (fig. 1). Our approach guarantees their positive definiteness. NCEP forecast on 6 hours on latitude–longitudinal grid with the steps $1^\circ \times 1^\circ$ was used as a first guess for the evaluations. Thus, we evaluate covariation for the difference between observations' data and the first guess. The archive of the data as well as forecast fields on territory to the north from 30° for 323 days was used for the evaluation. The evaluation has demonstrated (fig. 1) the essential distinctions between two CF for autocorrelation functions of temperature and a wind and insignificant — for all crosscorrelation and autocorrelations of a geopotential.

5. Methods of a combination of several (three) fields predictors were offered: we maximize L^2 difference between CF for two clusters (two points are separated or not separated by the frontal line).

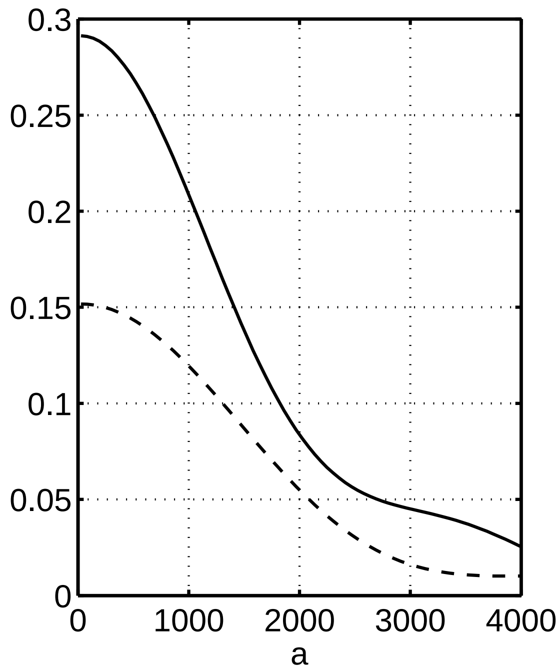

Fig. 1. Regular part of autocorrelation's functions on 300 gPa of difference between measurement and forecast a) temperature and b) geopotential for two clusters: i. two points are separated by the frontal line (dashed line) or ii. not separated (solid line). Horizontal axis — distance in kilometers. The CF may be represented as the sum $a\delta(x) + f(x)$, where $f(x)$ — is continues regular part, and $a + f(0) = 1$. The value $f(0)$ we obtain by an extrapolation from positive distances.

6. Clearness of atmospheric fronts grows with height, and the best quality is obtained at level of 300 gPa. It sharply falls on the levels about tropopause.

References

V.A.Gordin. Synoptical Situations Separate Correlation Functions. “Research Activities in Atmospheric and Oceanic Modeling" 27/865, pp. 1.25-1.26, (1998). O.A.Alduchov, V.A.Gordin. 3-D Correlation Functions of Basic Upper-Air Parameters. Izvestia of Russian Academy of Sciences. ser. “The Physics of Atmosphere and Ocean" , 2001, v.37, N 1, pp. 3-23 (Russian), 1-20 (English). V.A.Gordin Mathematical Problems and Methods in Hydrodynamical Weather Forecasting. — Amsterdam etc.: Gordon & Breach Publ. House, 2000. V.A.Gordin. Synoptical Situations Separate Correlation Functions. “Research Activities in Atmospheric and Oceanic Modeling" 27/865, pp. 1.25–1.26, (1998).

Nonlinear analysis of interaction between El Niño and Atlantic equatorial mode based on model simulations

S.S. Kozlenko[1], I.I. Mokhov[1], W.A.Mueller[2] and D.A.Smirnov[3]
[1]A.M. Obukhov Institute of Atmospheric Physics RAS, Moscow, Russia
[2]Max-Planck Institute for Meteorology, Hamburg, Germany
[3]Saratov Branch, V.A. Kotel'nikov Institute of RadioEngineering and Electronics RAS, Saratov, Russia
kozlenko@ifaran.ru

Interaction between processes in the tropical latitudes of the Pacific and Atlantic oceans with the help of nonlinear Granger causality and cross-wavelet analysis is analyzed. We use monthly mean indices for El Nino-Southern Oscillation (ENSO) and equatorial Atlantic mode (EAM) based on the data set for the model ECHAM5/MPI-OM since 1900 till 2100 (for the IPCC SRES scenario A1B for the 21st century). ENSO index is a sea surface temperature (SST) for Nino3.4 (5S-5N, 170W-120W), EAM index is SST for Atlantic3 (20W-0, 3S-3N) [Keenlyside and Latif, 2007].

The quantitative characteristic of the cause-and-effect relationship introduced by Granger is defined as the prediction improvement (PI) of one signal when another signal is taken into account in the predictive model [Granger, 1969]. Based on the nonlinear Granger causality analysis, statistically significant ENSO→EAM and EAM→ENSO influences without delay and with time delays of several months are detected. To assess changes in the interactions over time, the analysis in a 30-year moving window is performed (fig.1). We started with the interval 1900-1930 and finished with 2070-2100. The ENSO→EAM influence reaches its maximal value at the beginning of the twentieth century and greatly reduces over the next decade. The opposite influence at the beginning of the century is smaller, and at the end of the century is not detected. In the twenty-first century couplings in both directions are enhanced and reach maximum at the end of the century.

Cross-wavelet analysis [see Jevrejeva et al., 2003] reveals the existence of interaction between processes at different frequencies corresponding to periods from 2 to 10 years (fig.2). Interaction between the EAM and ENSO based on observational data set has already been analyzed in [Mokhov et al., 2007, Kozlenko et al., 2008]

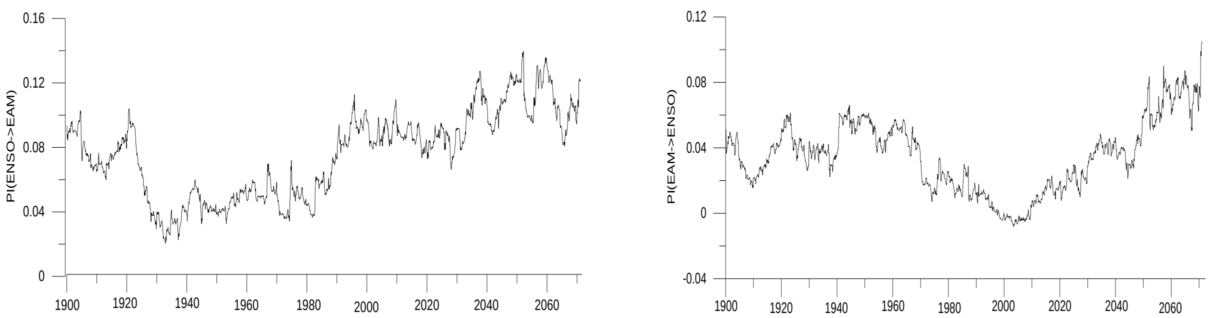

Fig.1.Influence EAM→ENSO (for zero trial time delay) in a 30-year moving window. Normalized values of prediction improvement are shown versus the start point of the moving window.

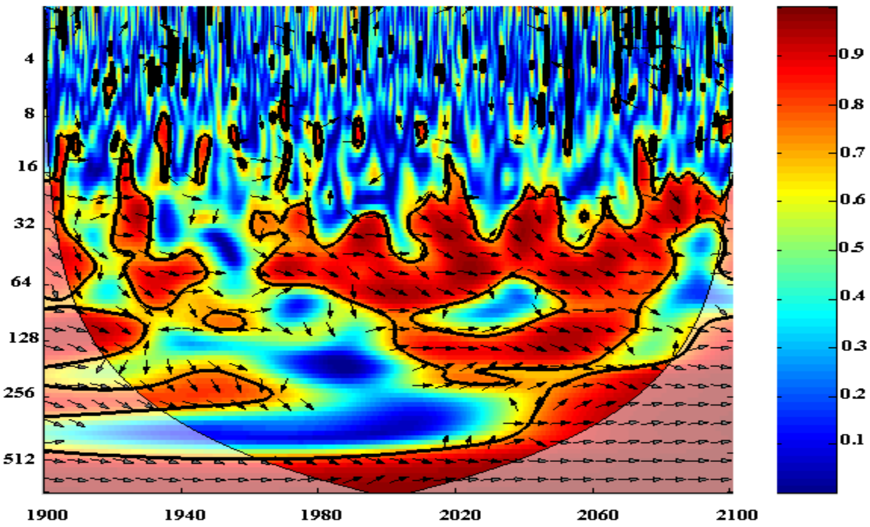

Fig.2. Cross-wavelet coherency between SSTs for Nino3.4 and Atlantic3.

References

Granger C.W.J. Investigating causal relations by econometric models and cross-spectral methods // *Econometrica*. 1969. V.37. P.424-438.

Jevrejeva S., Moore J.C., Grinsted A. Influence of the Arctic Oscillation and El Nino-Southern Oscillation (ENSO) on ice condition in the Baltic Sea: The wavelet approach // *J. Geophys. Res*. 2003. Vol.108. No.D21. 4677, doi:10.1029/2003ID003417.

Keenlyside N.S., and Latif M., Understanding Equatorial Atlantic Interannual Variability // *J. Climate*. 2007. 20, 131-142.

Kozlenko S.S., Mokhov I.I. and Smirnov D.A. Nonlinear analysis of interaction between El Niño and Atlantic equatorial mode // *Research Activities in Atmospheric and Oceanic Modelling*. Cote J. (ed.). Geneva: World Climate Research Programme. 2008. P.2-13.

Mokhov I.I., Bezverkhny V.A., Karpenko A.A., Keenlyside N.S., Kozlenko S.S. Cross-wavelet analysis of coherence and time lags between El Nino and Atlantic equatorial mode // *Research Activities in Atmospheric and Oceanic Modelling*. Cote J. (ed.). Geneva: World Climate Research Programme. 2007. P.2.19-2.20.

Muller W. A. and Roeckner E. ENSO impact on midlatitude circulation patterns in future climate change projections // *Geophys. Res. Lett.* 2006. Vol. 33. L05711, doi:10.1029/2005GL025032.

Frequency of extreme precipitation climate events over the Mediterranean region according to NNRP data for 1961-2000

Simon O. Krichak, Joseph S. Breitgand, Pinhas Alpert

Department of Geophysics and Planetary Sciences, Raymond and Beverly Sackler Faculty of Exact Sciences, Tel Aviv University
shimon@cyclone.tau.ac.il

Interannual variability of extreme precipitation events (Prec) over the Euro-Mediterranean region is investigated based on data on the number of days/month with extreme values of several atmospheric characteristics. The frequencies are calculated based on the NCEP/NCAR reanalysis daily 3D data from 1961 to 2000 available with 2.5 x 2.5 deg resolution. The daily data available from the NNRP dataset are complemented by 2D those on dynamic tropopause pressures (PDT). Frequencies of days with extreme values of the Prec, PDT and integrated water vapor (IWV) in each month of the 40 year period are then determined (Carril et al. 2008). Frequencies of days with the IWV values higher that 10 kg m^{-2}, are also calculated. Maps of spatial correlations between teleconnection indices of the NAO, EAWR, SCAND, NINO3.4 and EAWM with each of the three characteristics are constructed. The NAO, EAWR, SCAND and NINO3.4 time series used are those from the CPC NCEP website (http://www.cpc.noaa.gov/data/). Used in the analysis time series of the EAWM are calculated from the IWV frequency data using the EOF analysis approach to identify the area where the EAWM-associated extremes maximize.

Figs. 1a-d present the patterns with frequencies of extreme IWV days for September, November, January and March respectively. The eastern part of the Mediterranean region (EM) is found here in a zone with a low frequency of extreme IWV days. A gradual decrease in the frequency of extreme Prec from November to March may be noted over north-Africa. A rise in the number of days with extreme Prec events over the EM may be noted to the end of the cool season. The tendency (Figs. 2a-d) appears to be associated with an increase of contribution of the water vapor originating from the Indian Ocean area in the EM precipitation due to progress in formation of the Indian summer monsoon circulation patter to the end of cool season.

Acknowledgement: The research was supported by integrated project granted by the European Commission's Sixth Framework Programme, Priority 1.1.6.3 Global Change and Ecosystems (CIRCE), Contract no.:036961 and the Water Authority, Israel (Project No. 0603414981).

References:

Carril AF, S. Gualdi, A. Cherchi, A. Navarra (2008) Heatwaves in Europe: areas of homogeneous variability and links with the regional to large-scale atmospheric and SST's anomalies

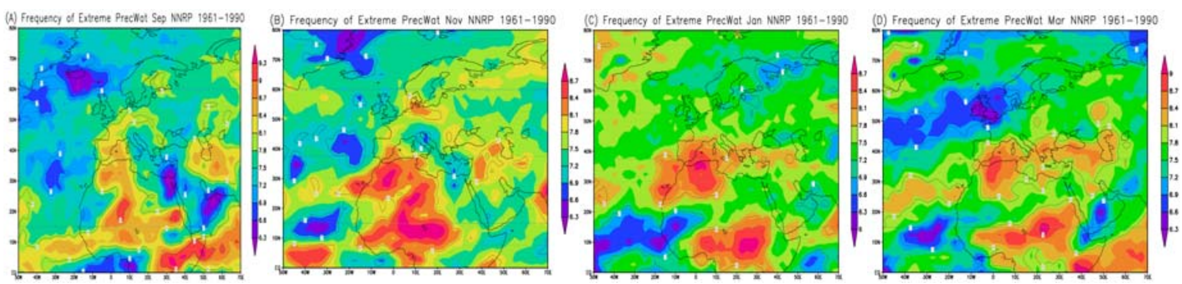

Fig. 1 Mean 40-years of days with extreme IWV values over the Euro-Mediterranean region during (a) September, (b) November, (c) January and (d) March,

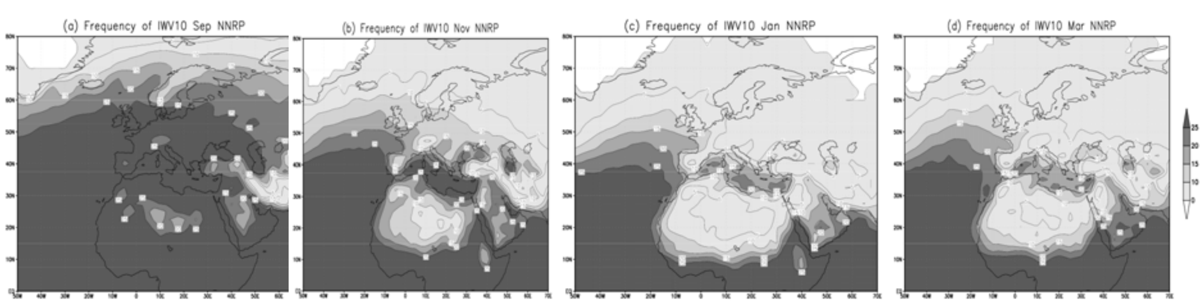

Fig. 2 Same as in Fig. 1, but for the days with IWV values greater than 10 kg m^{-2}

Trends in frequency of extreme precipitation climate events in the Mediterranean region according to NNRP data for 1961-2000

Simon O. Krichak, Joseph S. Breitgand, Pinhas Alpert

Department of Geophysics and Planetary Sciences, Raymond and Beverly Sackler Faculty of Exact Sciences, Tel Aviv University
shimon@cyclone.tau.ac.il

Evaluations of observation data demonstrate notable rise in the frequency and intensity of extreme precipitation events (EPE) over the globe. Significant parts of the Mediterranean region also seem to be experiencing the trend. Analysis of the issue represents a problem however since the region is not well enough covered by the observations. The paper presents results of application of a new approach (Carril et al. 2008) for investigation extreme events based on daily gridded data. The NCAR/NCEP data for 1961-2000 are used. Monthly data on the number of days with high values of integrated water vapor higher than 10 kg m^{-2} (IWV10) and 75 percentile of precipitation are obtained (Krichak et al. 2009). The IWV is used to account for synoptic situations characterized by narrow zones with strong meridional water vapor transport, which are contained within extratropical cyclone warm sectors ("atmospheric rivers", Neiman et al. 2008). Zhu and Newell (1998) showed that >90% of the meridional water vapor transport at midlatitudes takes place in atmospheric rivers. Linear trends of the EPE and IWV10 are computed by performing regression analysis in which the relationship between the number of EPE (or IWV10) days in a month and time is modeled by a least squares function. The analysis below is limited by the cool season months (September, November, January and March) only. Figs.1a-d present patterns with the IWV10 trends during September, November, January and March. Corresponding EPE patterns trends during the same months are given in Figs. 2 a-d, respectively. It may be noted that September – January period is characterized by a decline in the frequency of the EPE's over the Mediterranean region. A rise in the frequency of the EPE characterizes the region during March however whereas the negative trend zone is displaced to the southern Europe (Figs. 2a-d). The trends seem to be in good agreement with those in the IWV10 (Figs. 1a-d). Positioning of the zone with negative trend in the EPEs appears to be determined by intensity of positive trend in the frequencies of extreme IWV10 over central NH Africa – S. Asia and eastern Atlantic.

Acknowledgement: The research was supported by integrated project granted by the European Commission's Sixth Framework Programme, Priority 1.1.6.3 Global Change and Ecosystems (CIRCE), Contract no.:036961 and the Water Authority, Israel (Project No. 0603414981).

References:

Carril AF, S. Gualdi, A. Cherchi, A. Navarra (2008) Heatwaves in Europe: areas of homogeneous variability and links with the regional to large-scale atmospheric and SST's anomalies. Clim Dyn, 30, 77-98.

Krichak, S.O., P. Alpert, J. Breitgand (2009) Frequency of extreme precipitation climate events over the Mediterranean region according to NNRP data. Research Activities in Atmospheric and Oceanic Modelling, CAS/JSC WGNE, WMO (see this issue).

Neiman, P, FM Ralph, GA Wick, Y-H Kuo, T-K Wee, Z. Ma, GH Taylor (2008) Diagnosis of an intense atmospheric river impacting the Pacific northwest: storm summary and offshore vertical structure observed with COSMIC satellite retrievals. Mon. Wea. Rev., 136, 4398-4420.

Zhu, Y., R.E. Newell (1998) A proposed algorithm for moisture fluxes from atmospheric rivers. Mon. Wea. Rev., 725-735.

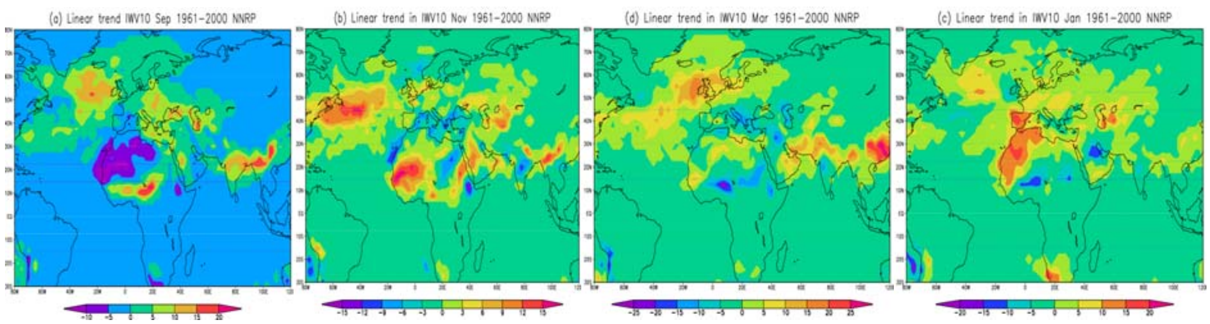

Figs 1. 40-y trend in frequency of IWV10 (a) Sept., (b) Nov., (c) Jan., (d) Mar

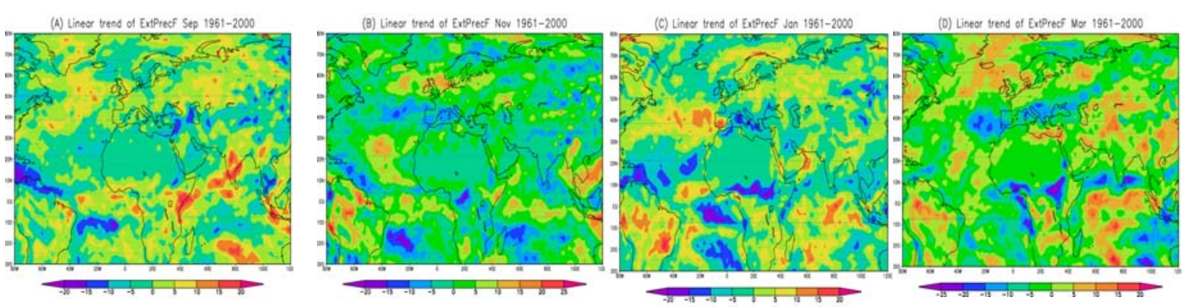

Figs.2. Same as in Figs. 1 but for EPE

Changes in action of atmospheric blockings

I.I. Mokhov, A.A. Vetrova

A.M. Obukhov Institute of Atmospheric Physics RAS, Moscow, Russia
mokhov@ifaran.ru

Changes in atmospheric blockings action *S* for the Northern Hemisphere during 1968-2007 were analyzed (Mokhov, 1999; Mokhov, 2006a,b).

Action *S* of individual climate structure, in particular for atmospheric blocking, is defined as $\int E(t)dt$, where integration on time *t* is performed from 0 to τ, τ – vortex life time, *E* – blocking energy. Kinetic energy of extratropical (geostrophical) vortex can be expressed via $(\Delta P)^2$, where ΔP is a pressure difference between centre and periphery of the vortex (Akperov et al., 2007; Golitsyn et al., 2007). Integral action S_Σ for ensemble of vortices is defined by the sum of values of action for individual vortices.

Action *S* of individual blockings was estimated as proportional to $I^2\tau$ with mean intensity I (I related with ΔP) and duration τ of blocking determined according to Wiedenmann et al. (2002).

Figure 1 shows changes of atmospheric blockings action *S* (normalized on the mean value for 1971-2000) in the Northern Hemisphere during 1968-2007 for annual means, winter and summer. General increase of *S* during last decades is accompanying by significant interannual variations especially during last years. Tendency of the increase during last decades (at least since1980s with a general warming) was obtained in the Northern Hemisphere for all seasons but with different level of significance. The most significant trend of *S* was estimated for spring season.

It should be noted that the most significant mean contribution to the annual blockings action is associated with winter season. The least values of *S* were obtained for summer season. Extreme value of S in summer was noted in 2003. This summer was extremely warm in Europe (with drought and fire conditions related with blocking conditions).

This study was supported by the RFBR and RAS programs.

References

Akperov, M.G., M.Yu. Bardin, E.M. Volodin, G.S. Golitsyn, and I.I. Mokhov, 2007: Probability distributions for cyclones and anticyclones from the NCEP/NCAR reanalysis data and the INM RAS climate model. *Izvestiya, Atmospheric and Oceanic Physics,* **43**, 705–712.

Golitsyn G.S., I.I. Mokhov, M.G. Akperov, and M.Yu. Bardin, 2007: Distribution functions of probabilities of cyclones and anticyclones from 1952 to 2000: An instrument for the determination of global climate variations. *Doklady Earth Sciences,* **413**, 324–326.

Mokhov, I.I., 1999: Blocking activity in Northern Hemisphere: Detection of change and attribution of causes. Proc. 4th Intern. Conf. on Modelling of Global Climate Change and Variability, MPI, Hamburg, 223.

Mokhov, I.I., 2006a: Action as an integral characteristic for climatic structures: Estimates for atmospheric blockings. *Research Activities in Atmospheric and Oceanic Modelling,* J. Cote (ed.). Geneva: WCRP. WMO TD-No.1347. Section 2, 27-28.

Mokhov, I.I., 2006b: Action as an integral characteristic of climatic structures: Estimates for atmospheric blockings. *Doklady Earth Sciences,* 2006, **409A**, 925–928.

Wiedenmann, J.M., A.R. Lupo, I.I. Mokhov, and E.A. Tikhonova, 2002: The climatology of blocking anticyclones for the Northern and Southern Hemispheres: Block intensity as a diagnostic. *J. Climate*, **15**, 3459-3473.

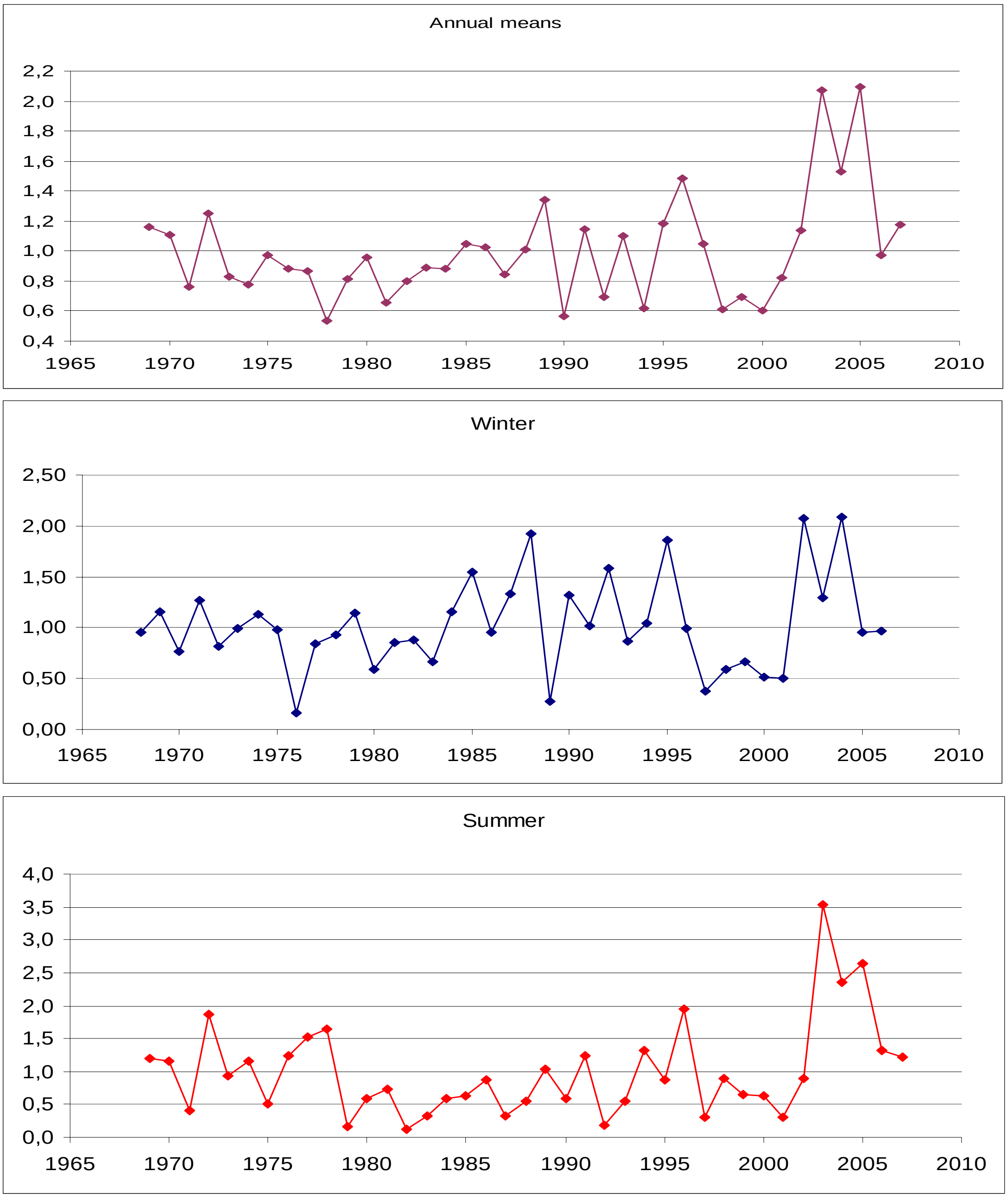

Figure 1. Changes of atmospheric blockings action (normalized on the mean value for 1971-2000) in the Northern Hemisphere during 1968-2007 for annual means (a), winter (b) and summer (c).

WGNE Intercomparison of Tropical Cyclone Forecasts using Operational Global Models

Hirokatsu Onoda and Takuya Komori
Numerical Prediction Division, Japan Meteorological Agency
1-3-4 Otemachi, Chiyoda-ku, Tokyo 100-8122, Japan
(E-mail: h.onoda@met.kishou.go.jp, komori@met.kishou.go.jp)

1. Introduction

The CAS/JSC Working Group on Numerical Experimentation (WGNE) has conducted intercomparison of Tropical Cyclone (TC) track forecasts using operational global models since 1991. WGNE recognizes that the evaluation of TC track forecasts can indicate the performance of such models in the tropics and subtropics.

2. Dataset

The verification area is divided into six regions according to the domains of responsibility for each TC RSMC and the best track data offered by each RSMC is used for verification. This report describes the results for the western North Pacific. Table 1 shows the specifications of the data provided by NWP centers, including model resolutions and the usage of TC bogus data in the analysis system.

Table 1 Specifications of data offered in verification of 2007

NWP center	Model	Data res.	Bogus
JMA (Japan)	TL319L40	1.25×1.25	use
ECMWF (Europe)	TL799L91	0.25×0.25	—
Met Office (UK)	0.38×0.56L50	0.38×0.56	use
CMC (Canada)	0.9×0.9L58	1.0×1.0	—
DWD (Germany)	40kmL40	0.5×0.5	—
NCEP (USA)	T382L64	1.0×1.0	use
BoM (Australia)	TL239L60	0.75×0.75	—
Météo France	TL358L46	0.5×0.5	use
NRL (US Navy)	T239L30	1.0×1.0	use

3. Verification using MSLP(mean sea level pressure) data

The verification method of Sakai and Yamaguchi (2005) is adopted in this study. The performance of TC track forecasts is evaluated using position errors and detection rates. The detection rate is defined as A(t)/B(t).

- A(t) : The number of forecast events in which a TC is analyzed at forecast time T on the condition that the model continuously expresses the TC until the forecast time t.
- B(t) : The number of forecast events in which a TC is analyzed at forecast time t.

The position error growth by forecast time is shown in Fig.1. Figure 2 shows the mean position errors and detection rates of the participating global models for 72-hour forecasts. It can be seen that NCEP is the best in terms of position error, but demonstrates a medium level of performance in detection rate.

We also investigate the prediction of TC genesis. The minimum MSLP point is ascertained from the time of genesis using the backtracking method. Figure 3 shows a bar chart of the forecast lead time of each center for all TCs in 2007. The term *lead time* refers to the length of the forecast that first captures the corresponding TC genesis in advance of the actual TC genesis. NARI(T0711) and TAPAH(T0722) are examples in which genesis forecasting was difficult for all centers. Further investigation will be necessary on the differences in difficulty of forecasting among TC geneses.

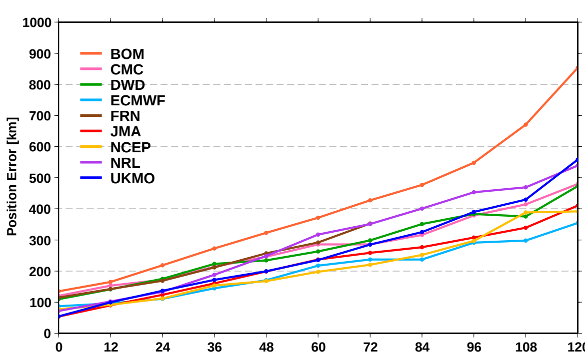

Fig 1 The position error growth in western North Pacific.

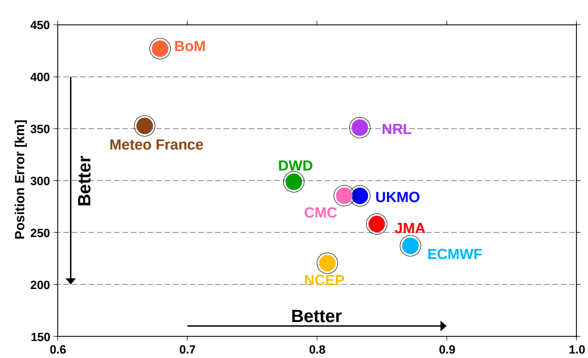

Fig 2 A relation of position error and detection rate of 72-hour forecast.

Reference

Tsuyuki, T. et al., 2002: The WGNE intercomparison of typhoon track forecasts from operational global models for 1991-2000. WMO-BULLETIN, vol.5, No.3, 253-257.

Sakai, R., and M. Yamaguchi, 2005: The WGNE Intercomparison of Tropical Cyclone Track Forecasts by Operational Global Models. CAS/JSC WGNE Research Activities in Atmospheric and Oceanic Modeling, Report No.35, Jul 2005, WMO/TD-No.1276, 2.7-2.8.

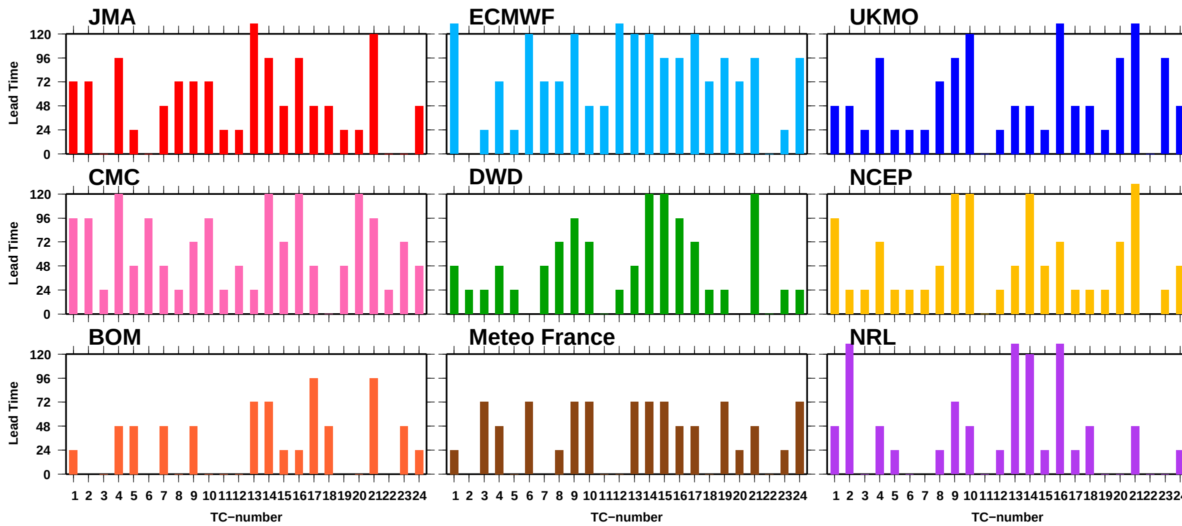

Fig 3 The lead time of the forecast for all TC geneses in western North Pacific in 2007. The protruded bar shows lead time is longer than 120 hours.

4. Verification of the axi-symmetric wind structure of TCs using wind data

We examine the characteristics of the stability structure of TCs using wind data which were offered by seven centers except DWD and NCEP. The average radial wind is calculated by averaging wind data for each point P(r,θ) (distance r is set every 25km, and angle θ is set every 2° from the TC center) in concentric circles. A schematic explaining the averaging method is given in Fig.4. It should be noted that the average depends on the horizontal resolution of the data. KROSA(T0715), which had comparatively concentric circle shapes with minimal topographical influence, was selected for verification. Changes in wind structure by initial time are examined in Fig.5, in which forecasts of TC wind structure from four different initial times with 24-h intervals are compared. Red line shows KROSA's structure in the analysis by each model at 12UTC 5 October 2007. And other colored lines show 24, 48, 72, 96-hour forecasts of wind structure, all valid for the same analysis time. In this particular case, BoM, CMC, JMA and NRL show relatively large changes in TC structure among initial times.

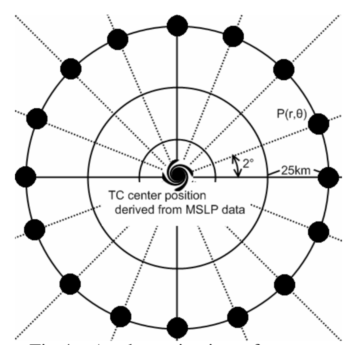

Fig 4 A schematic view of average radial wind.

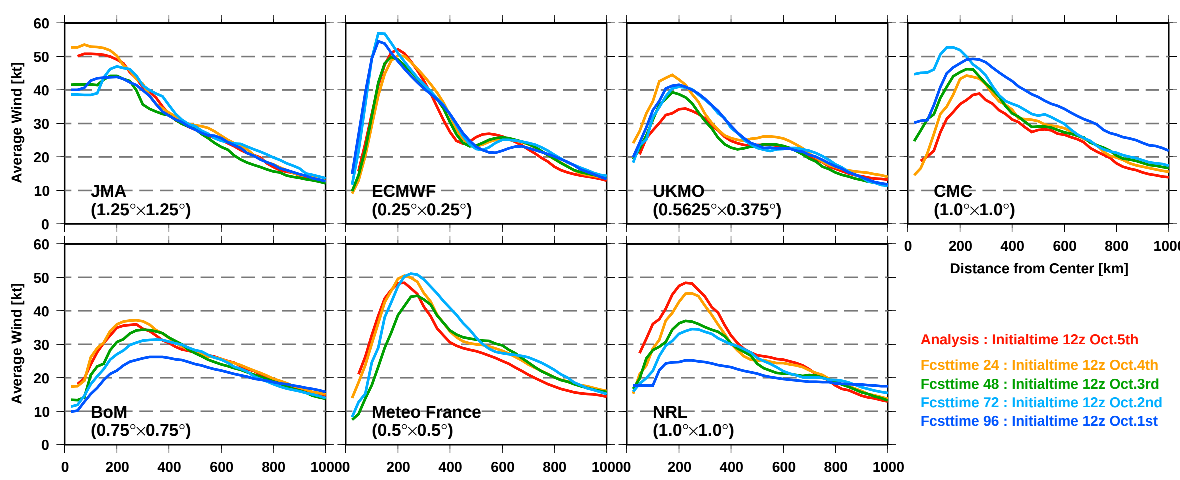

Fig 5 The average radial wind distribution of the radius vector direction of KROSA at 12UTC 5 October 2007. Red line means analysis at 12UTC 5 October, and other colored lines mean forecast from 4 days ago.

About possible variants of the development of the atmosphere unstable states

Pokhil A.E.*, Margolin A.D.**

* The Hydrometcentre of Russia, 123242 Moscow, B. Predtechenskiy per. 9-11. E-mail: Pokhil@mecom.ru
** The Institute of Chemical Physics of the Russian Academy of sciences

In the dynamics of the atmosphere of our planet there occur unpredictable situations, when synoptic processes can develop in different ways with equal probability. In this work the variants of the development of such unstable situations are studied using the numerical model by Zlenko (1987). Ensembles of vortices of finite dimensions are considered, characterized by identical velocity fields and different directions of rotation – cyclones (C) and anticyclones (AC), the distance between them being comparable with their dimensions. The calculations by Pokhil et al. (1991 – 2000) provide information about the interaction of the vortices: about their moving apart, drawing together, fragmentation, changes in their dimensions and form, and about specific cases of sharp change in their behaviour.

The interaction of distributed vortices is examined in the perfect liquid. Note that the interaction of vortices in the perfect liquid ($Re = \infty$) practically does not differ from their interaction in the viscous liquid at
$R > 100$.

The wind velocity tangential component profile in the experiments is as follows:

$$V(r)=V\,(r/R)\exp[1/b\cdot(1-(r/R)^b)]$$

where r is the distance from the vortex centre; V is the maximum of the tangential component of the wind velocity; R is the distance at which V is reached; b is the parameter characterizing the change of the wind velocity tangential component in the radial direction (b = 2). Numerical experiments were performed with vortices located in the apexes of polygons, where the nearest neighbours were vortices of different signs. The integer angular momentum was equal to zero.

The dynamics of four vortices located in the apexes of a square. At the initial relative distance between the centres of the neighbouring vortices (C and AC) $d/R > 6$ these vortices don't interact in the numerical experiment ($T = 17$). Nevertheless, even in the case of vortices quite distant from one another the interaction can start after a while, because in the rear of the vortex an area of vorticity of opposite sign forms, which, getting larger, reaches the neighbouring vortex and starts interacting with it (Fig. 1); another reason can be the instability of the velocity sharp decrease at $r > R$ and gradual "spreading out" of the vortex peripheral part.

At shorter distances ($d/R \sim 3$-6) the group splits into two pairs moving in the opposite directions (Fig. 1). In the rear of the pairs a cloud of small vortices forms, which is typical of distributed vortices. At $d/R_o < 1$ a so-called "two-headed" vortex forms whose centre of gravity is precessing. Such vortices are observed in nature and have been obtained using a numerical model (Pokhil, 1996).

The dynamics of four vortices located in the apexes of a rhomb (Fig. 2). In the performed experiments at an insignificant change of d one could observe different kinds of interaction, with the vortices following different tracks. In Fig. 2, after the central vortices merge into a big vortex, secondary vortices start interacting with quite distant peripheral ones. This is the cause of spiral-shaped trajectories of the peripheral vortices (Fig. 2 g).

The dynamics of the ensembles of six vortices located in the apexes of a regular hexagon. In the case of certain specific relationships between the parameters of vortices and the distances between them a group of vortices splits into three pairs, which move away from the centre, in the ideal case, at an angle of 120º.
If at the beginning of the experiment the vortices are located close to each other in one of the pairs (or if they are located far from other vortices), the dynamics of the vortices is such as is shown in Fig.4.

Conclusions.

1. The evolution of a group of vortices rotating in dissimilar ways can follow different scenarios: with insignificant change of the system parameters one can make the vortices rotate with respect to one another in a cyclonic and in an anticyclonic way and make them move in different directions.
2. Under certain conditions the interaction of vortex systems is accompanied by the formation of a cloud of secondary small vortices, which, while interacting with the initial vortices, can substantially change their behaviour.

References

1. Zlenko V.A., 1987: Hydrodynamical scheme of the calculation of tropical cyclones tracks. – Meteorology and Hydrology, No. 5, 56-61.
2. Pokhil A.E., 1991: About the origination and destruction of secondary vortices in the course of the interaction of two tropical cyclones. – Meteorology and Hydrology, No. 9, 56-61.
3. Pokhil A.E., 1996: About some conditions of the formation of a great vortex and the characteristic features of the interaction of vortices. – Meteorology and Hydrology, No. 2, 24-32.
4. Pokhil A.E., Poliakova I.V., 1994: About the influence of the structure of the interacting vortices on their motion. – Meteorology and Hydrology, No. 7, 17-23.
5. Pokhil A.E., Sitnikov I.G., Galkin S.A., 1997: The interaction of three ideal vortices in a numerical model and the behaviour of a group of real tropical cyclones in the Pacific. – Meteorology and Hydrology, No. 2, 28-32.
6. Pokhil A.E., Sitnikov I.G., Zlenko V.A., 2000: About the behaviour of solitary cyclonic and anitcyclonic vortices and their interaction in homogeneous fields taking into account and without taking into account the beta-effect. – Meteorology and Hydrology, No. 9, 39-48.

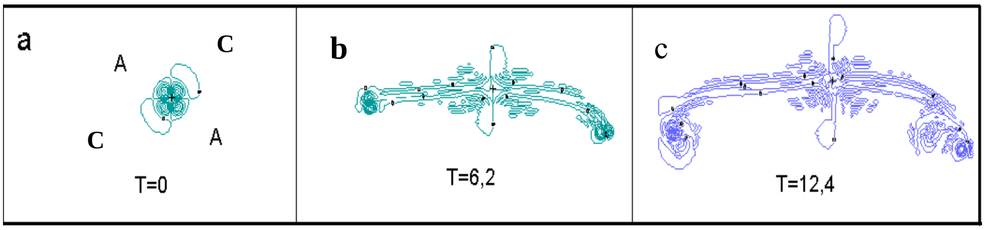

Fig. 1, a,b,c. The evolution of the vorticity fields of 4 interacting vortices of different signs (2 cyclones and 2 anticyclones). The initial relative distance between the vortices d/R=4
f) the tracks of the vortices (the initial positions of the vortices are marked by squares).

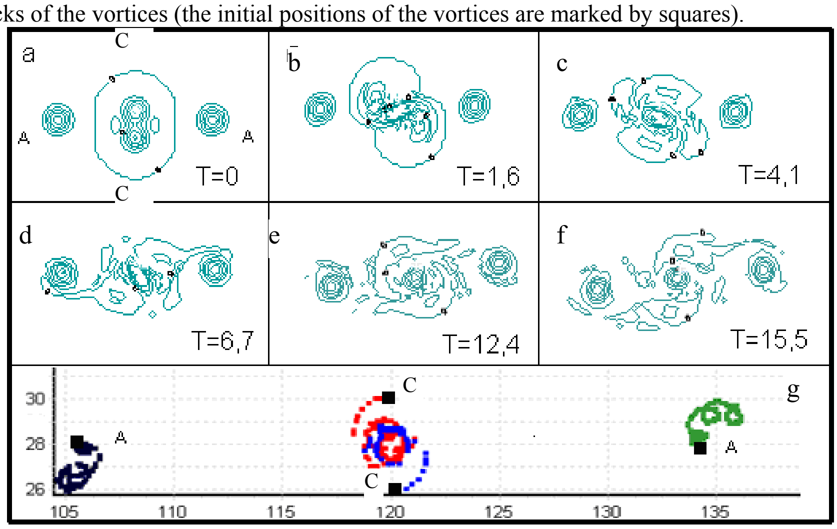

Fig. 2 a,b,c,d,e,f. The evolution of the vorticity fields of 4 interacting vortices of different signs (2 cyclones and 2 anticyclones). The initial relative distance between the central vortices d/R_C=2.2, between the central and the peripheral vortices d/R_{CP}=6.8; g) the tracks of the vortices (the initial positions of the vortices are marked by squares).

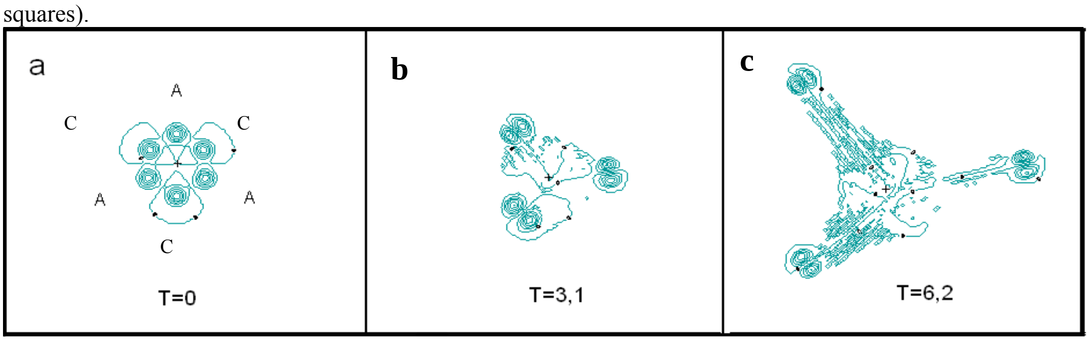

Fig.3 a,b,c. The evolution of the vorticity fields of 6 interacting vortices of different signs (3 cyclones and 3 anticyclones). The initial relative distance between the central vortices d/R~3.35.

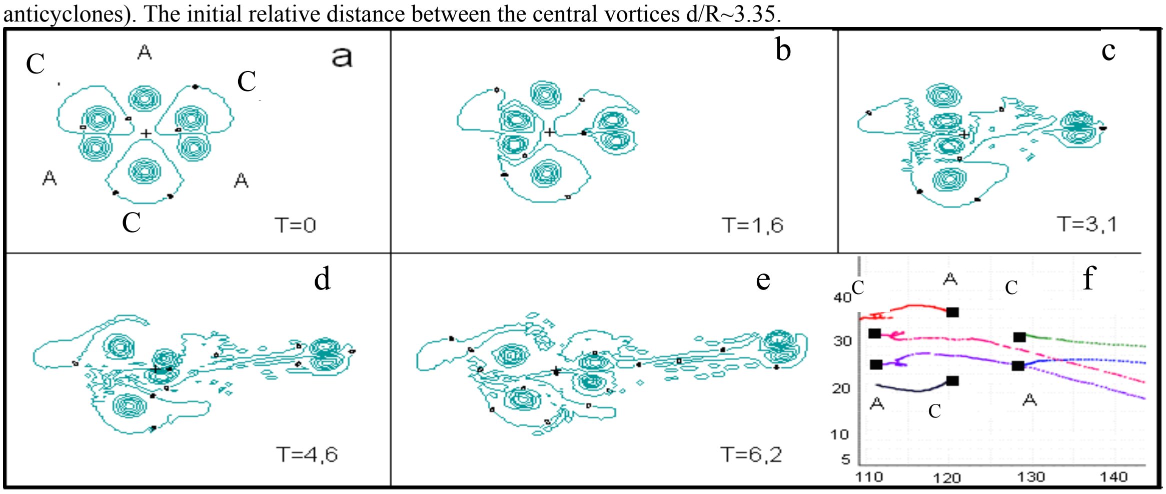

Fig. 4 a,b,c,d,e,f. The evolution of the vorticity fields of 6 interacting vortices of different signs (3 cyclones and 3 anticyclones). The initial relative distance between the vortices of the right-hand pair d/R~3.25 is less than that between the others. g) the tracks of the vortices (the initial positions of the vortices are marked by squares).

About the formation of a cloud of small vortices in the case of the interaction of a few larger vortices of finite dimensions.

Margolin A.D.**, Pokhil A.E.*

* The Hydrometcentre of Russia, 123242 Moscow, B. Predtechenskiy per. 9-11. E-mail: Pokhil@mecom.ru
** The Institute of Chemical Physics of the Russian Academy of sciences

Numerical modeling (Pokhil et al. 1991-2006) shows that the interaction of vortices is accompanied by the formation of secondary smaller vortices. Let's estimate approximately the number and the total mass of the obtained small vortices reasoning from the laws of conservation of mass, the moment of momentum and energy.

In real atmospheric vortices the Reynolds number is great ($Re>10^7$). We will assume that the energy dissipation during the interaction of vortices that is studied here can be neglected. The vortex effective mass is proportional to ρR^2, the moment of momentum – to $\rho R^3 V$, the energy – to $\rho R^2 V^2$ (ρ is the density). The calculation of the energy and moment of momentum reduces to the calculation of convergent integrals in the case of a sufficiently strong function of the wind velocity decrease at $r>R$, e.g. the exponential one. The vortex effective mass will be considered as the mass of the area that contributes to the vortex moment of momentum most (for example, 0.9). We will also assume that all the vortices have identical wind velocity profile $V(r)/V=f(r/R)$. If n_1 identical vortices with the radius R_1 draw together and as a result it remains (or there forms) n_2 identical vortices with identical rotation and with the radius R_2, and also it forms n_3 small vortices with the radius R_3, the conservation laws take the form

$$n_1R_1^2=n_2R_2^2+n_3R_3^2$$
$$n_1R_1^3V_1=n_2R_2^3V_2-n_3R_3^3V_3 \qquad (1)$$
$$n_1R_1^2V_1^2=n_2R_2^2V_2^2+n_3R_3^2V_3^2$$

It is assumed that the velocity of the vortices' motion is substantially less than the velocity of wind V in them and that the radius of small vortices is substantially less than that of the main vortices.

1. If the wind velocities in the small vortices are little, these vortices contribute to the overall energy and to the moment of momentum only slightly. Taking this into account we obtain that the relative mass m_3/m_1 of the vortices that have formed vs. the mass of the initial vortices and their relative number n_3/n_1 take the form

$$m_3/m_1= 1-(n_2/n_1)^{1/2}; \quad n_3/n_1 = (1-(n_2/n_1)^{1/2})(R_1/R_3)^2 . \qquad (2)$$

The radius R_2 and the wind velocity V_2 of the newly formed great vortices just slightly depends on the number of these vortices, because $R_2/R_1 = V_2/V_1 = (n_1/n_2)^{1/4}$. The relative mass of the "great" vortices that have formed is then

$$m_2/m_1= n_2R_2^2/n_1R_1^2=(n_2/n_1)^{1/2}.$$

It is easy to see that we obtain a positive solution only in the case of $n_2/n_1<1$. When $n_2=2$ and $n_2=1$, 0.3 of the mass of initial vortices passes into small vortices.

2. If $V_2/V_1=1$, then small vortices contribute to the overall energy to the extent comparable with the full energy, and to the moment of momentum they contribute to a small extent, because $R_3<<R_1$. In this case we obtain

$$m_3/m_1=1-(n_2/n_1)^{1/3}; \quad n_3/n_1=(1-(n_2/n_1)^{1/3})(R_1/R_3)^2 \qquad (3)$$
$$V_2/V_1=1; \quad R_2/R_1=(n_1/n_2)^{1/3}$$

At $n_1=2$ and $n_2=1$ the mass of small vortices is equal to ~0.2 of the mass of the initial vortices.

Thus, the overall mass of small vortices is just slightly dependent on the maximum wind velocity in them. Furthermore, all the presented results practically do not depend on the sign of the small vortices and remain unchanged if there are small vortices of different signs as well.

3. Suppose that, while interacting, several like vortices split into two groups of small vortices, with one of them forming a "compound" central vortex consisting of a multitude of small vortices and the second one forming a cloud of comparatively slow-moving vortices as compared to the maximum wind velocity in the initial vortices (Pokhil et al. 1991-1997). Let's assume that in the central vortex that has formed small vortices are distributed uniformly, so that the mean density of matter in the "compound" vortex is constant and $\rho_2<\rho_1$, where ρ_1 is the matter density in the initial vortices, ρ_2 is that in the resulting compound vortices. Furthermore, let's suppose that the wind velocity in all the small vortices and the velocity of any motion of the vortices of the second group are considerably less than the maximum wind velocity in the resulting "compound" vortices of the second group. On these assumptions the conservation equations remain the same as in the second case, if in these equations we change n_2 for $n_2 \cdot \rho_2/\rho_1$. So, the radius of the obtained compound vortices is R_2, the maximum velocity in them is V_2 and the relative mass and the number of small vortices will be equal to

$$m_3/m_1 = 1-\sqrt{(n_2\rho_2)/(n_1\rho_1)} \quad ; \quad R_2/R_1= V_2/V_1 = (n_1\rho_1/n_2\rho_2)^{1/4} \qquad (4)$$
$$n_3/n_1 = (1-\sqrt{n_2\rho_2 \cdot n_1\rho_1})(R_1/R_3)^2 \quad ;$$

Here, as in the previous case that we have considered, n_1 is the number of initial vortices, n_3 is the number of small vortices of the group, R_3 is their radius.

In the case under consideration we obtain positive solutions at $n_2\rho_2/n_1\rho_1<1$, i.e. it is allowed that the number of the obtained compound vortices would be equal or would even exceed the number of initial continuous vortices. If out of two initial vortices one "compound" vortex forms, its mass constitutes a minor part of the mass of initial vortices.

It should be noted that the effective density ρ_2 of the compound vortex has a minor effect on its diameter and velocity.

4. It was supposed above that the wind velocity profile in the newly formed and initial vortices is identical. If the profile of the wind velocities does not change while identical vortices with identical rotation interact, a cloud of small vortices ($R_3/R_1<<1$) can form only if after the interaction the number of identical vortices formed after the interaction is less than that of the initial vortices. Nevertheless, numerical modeling shows that in the case of the interaction of two identical vortices with identical rotation both vortices can remain unchanged, forming at the same time a cloud of small vortices (Pokhil et al. 1991-2006).

In connection with such observations let's examine the interaction n_1 of identical vortices with identical rotation, from which results the formation of "great" and "small" vortices, with the wind velocity profile in the vortices becoming other than before the interaction. The interaction results in the formation of n_2 "large" vortices comparable with the initial ones, and in the formation of n_3 "minor" vortices whose radius is less than that of the initial vortices. Let's assume that the small vortices are characterized by a little velocity $V_3/V_1<<1$. Suppose that the mass, the moment of momentum and the energy of the initial and the newly formed vortices, taking into account the change of the wind profile after the interaction, are as follows:

mass – $\alpha_i \rho R_i^{\,2}$

the moment of momentum – $\beta_i \rho R_i^{\,3} V_i$ (5)

energy – $\gamma_i \rho R_i^{\,2} V_i^2$, where α_i, β_i, γ_i depend on the distribution of the wind velocities.

Then the conservation laws at $R_3/R_1<<1$ and $V_3/V_1<<1$ take the form:

$$\alpha_1 n_1 R_1^{\,2} = \alpha_2 n_2 R_2^{\,2} + \alpha_3 n_3 R_3^{\,2} \qquad (6)$$
$$\beta_1 n_1 R_1^{\,3} V_1 = \beta_2 n_2 R_2^{\,3} V_2$$
$$\gamma_1 n_1 R_1^{\,2} V_1^2 = \gamma_2 n_2 R_2^{\,2} V_2^2$$

Having solved the equations we will obtain that the relative masses of the originated "large" and "minor" vortices are equal to:

$$m_2/ m_1= (\alpha_2/\alpha_1)\,(\beta_1/ \beta_2)\,(\gamma_2 / \gamma_1)^{1/2}(n_2/ n_1)^{1/2} \quad \text{и}$$
$$m_3/ m_1= 1- (\alpha_2/\alpha_1)\,(\beta_1/ \beta_2)\,(\gamma_2 / \gamma_1)^{1/2}(n_2/ n_1)^{1/2}\,; \qquad (7)$$

If the coefficient $(\alpha_2/\alpha_1)\,(\beta_1/ \beta_2)\,(\gamma_2 / \gamma_1)^{1/2} <1$, then the cloud of small vortices can form at $n_3/n_1=1$, i.e. if the number of originated "large" vortices is the same as in the initial case.

Such a situation occurs if the originating "large" vortices are characterized by a more sharp velocity drop than the initial vortices.

5. If it is the case of the interaction of vortices with different rotation, whose total the moment of momentum is equal to zero, the conservation laws restrict the parameters of the originated vortices to a lesser extent than in the case of the interaction of the vortices with identical rotation.

In case if slow-moving ($V_3/V_1<<1$) small vortices are formed, the conservation laws are as in (6); with the difference that the total the moment of momentum is equal to zero.

Let's consider a most simple case when out of two vortices with different rotation form two vortices also with different rotation, with the characteristic radii of all the four vortices being equal, and, besides that, the interaction results in the formation of small vortices with $R_3/R_1<<1$ and $V_3/V_1<<1$. In this case

$$2\,\alpha_1 R_1^2=2\,\alpha_2 R_2^2 + n_3\,\alpha_3 R_3^2$$

Taking into account that, by the data, , we obtain

$$m_2/ m_1= (\alpha_2/\alpha_1)\,(R_2/R_1)^2= \alpha_2/\alpha_1 \quad \text{и} \qquad (8)$$
$$m_3/ m_1=(\alpha_3/\alpha_1)(n_3/ n_1)\,(R_3/R_1)^2 = 1- \alpha_2/\alpha_1, \qquad (9)$$

that is, a cloud of small vortices forms when the velocity drop becomes sharper.

References

1. Alexeenko S.V., Kuibin P.A., Okulov V.L. 2003: Introduction to the theory of concentrated vortices. Novosibirsk, 503 p.
2. Borisov A.I., Mamaev I.S. Mathematical methods of the dynamics of vortical structures. Moscow Izhevsk, 2005.
3. Pokhil A.I. 1991: About the origination and destruction of secondary vortices in the course of the interaction of two tropical cyclones. Meteorology and Hydrology, No. 9, 34-41.
4. Pokhil A.E., 1996: About some conditions of the formation of a great vortex and the characteristic features of the interaction of vortices. Meteorology and Hydrology, No. 2, 24-32.
5. Pokhil A.E., Sitnikov I.G., Galkin S.A., 1997: The interaction of three ideal vortices in a numerical model and the behaviour of a group of real tropical cyclones in the Pacific. Meteorology and Hydrology, No. 2, 28-32.
6. Pokhil A.E., Speranskaia A.A. 2006: Study of tropical cyclones in real conditions and using laboratory modeling. Meteorology and Hydrology, No. 7, pp.16-23.

Estimation of extratropical cyclone characteristics from station data

David Kent and Ian Simmonds

School of Earth Sciences, The University of Melbourne
Victoria, 3010, Australia
simmonds@unimelb.edu.au

Our group is experimenting with algorithms designed to diagnose the nature of 'nearby' extratropical cyclones solely from station data. The diagnosis of cyclone characteristics from quality analyses (such as reanalyses) is an important tool for the climatologist. Having said that it is known that the various reanalysis sets have artificial trends of various types, and the length of reliable record is relatively short, particularly in the Southern Hemisphere. Hence diagnosing cyclone climate variability and trends with these must be undertaken with caution. A useful complement to such approaches is to attempt to diagnose 'nearby' cyclones from station data.

A number of measures of 'storminess' have been developed using station data (e.g., Wang et al. (2006). We report on a novel approach, which we exemplify for the station records at Melbourne. From the NCEP2 reanalysis for the period 1979-2008 we determine with The University of Melbourne cyclone identification algorithm (Simmonds et al. 2003, Lim and Simmonds 2007) the times when a cyclone centre was in the proximity of Melbourne. We show a test case where 'near' means cyclone centres lie within 142.5-147.5°E, 50-37.5°S. 190 extratropical cyclone events were so-identified. For each of these events we extracted the four (3-hourly) Melbourne pressure observations for the 12-hour periods prior to and after the time of cyclone identification. The structures of these 24-hour pressure traces (represented as anomalies from their individual means) can be used to diagnose nearby cyclonic behaviour. Here we show the simple case of compositing all the traces into one 'characteristic' sequence, which is shown in Fig. 1. In this simplest case, one can say that if a given pressure anomaly sequence is a 'close' fit to the characteristic sequence then there is a cyclone in the vicinity. A fit is said to be close if the RMS difference is less than a prescribed amount.

Fig. 2(a) shows the distribution of the pressure anomalies averaged over all the cases when cyclones were in the target area defined above. Fig. 2(b) shows a similar composite but, this for the times identified as close matches to the 'characteristic sequence'. The presence of a significant pressure minimum very similar to that in part (a) indicates that the method does in fact identify times when extratropical cyclone activity is present. Further details can be found in Kent (2008). We have described here a very simple version of our scheme. Work is continuing on making use of synoptic-typing options and on transportability to very different environments.

Kent, D., 2008: Estimation of Extratropical Cyclone Characteristics from Station Data. Honours thesis, School of Earth Sciences, The University of Melbourne, 38 pp.

Lim, E.-P., and I. Simmonds, 2007: Southern Hemisphere winter extratropical cyclone characteristics and vertical organization observed with the ERA-40 reanalysis data in 1979-2001. *J. Climate*, **20**, 2675-2690.

Simmonds, I., K. Keay and E.-P. Lim, 2003: Synoptic activity in the seas around Antarctica. *Mon. Wea. Rev.*, **131**, 272-288.

Wang, X. L., H. Wan and V. R. Swail, 2006: Observed changes in cyclone activity in Canada and their relationships to major circulation regimes. *J. Climate*, **19**, 896-915.

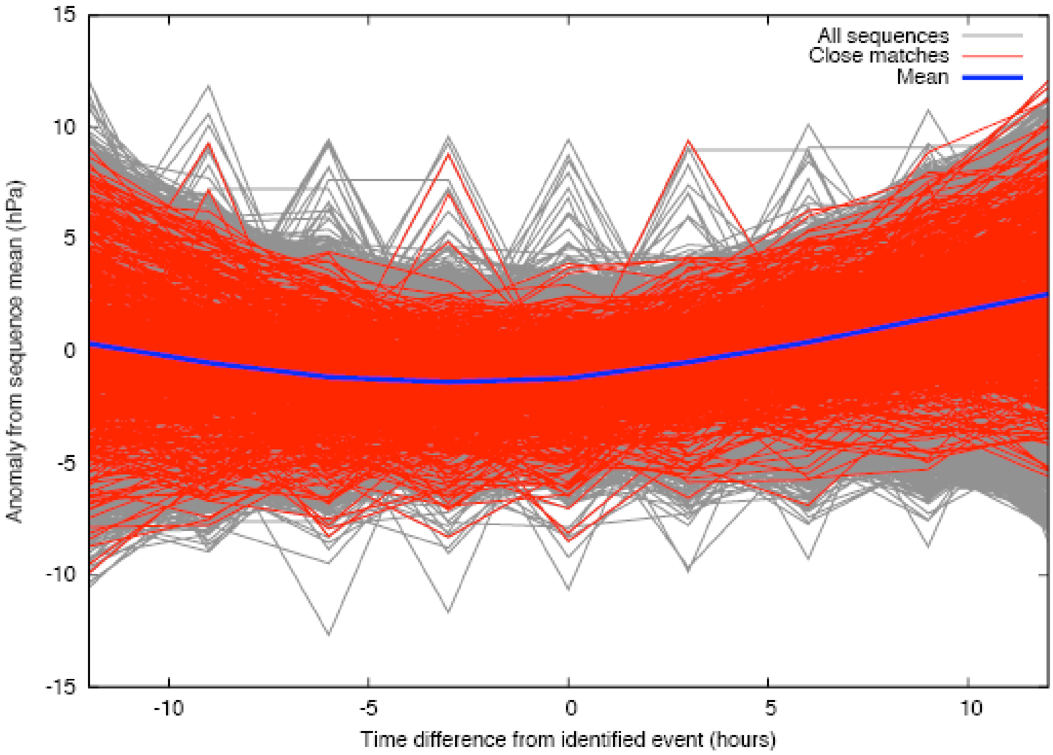

Fig. 1: Extracted pressure sequences for Melbourne, with . Blue line is mean sequence presented in blue). (The grey lines have large RMS difference from the mean.)

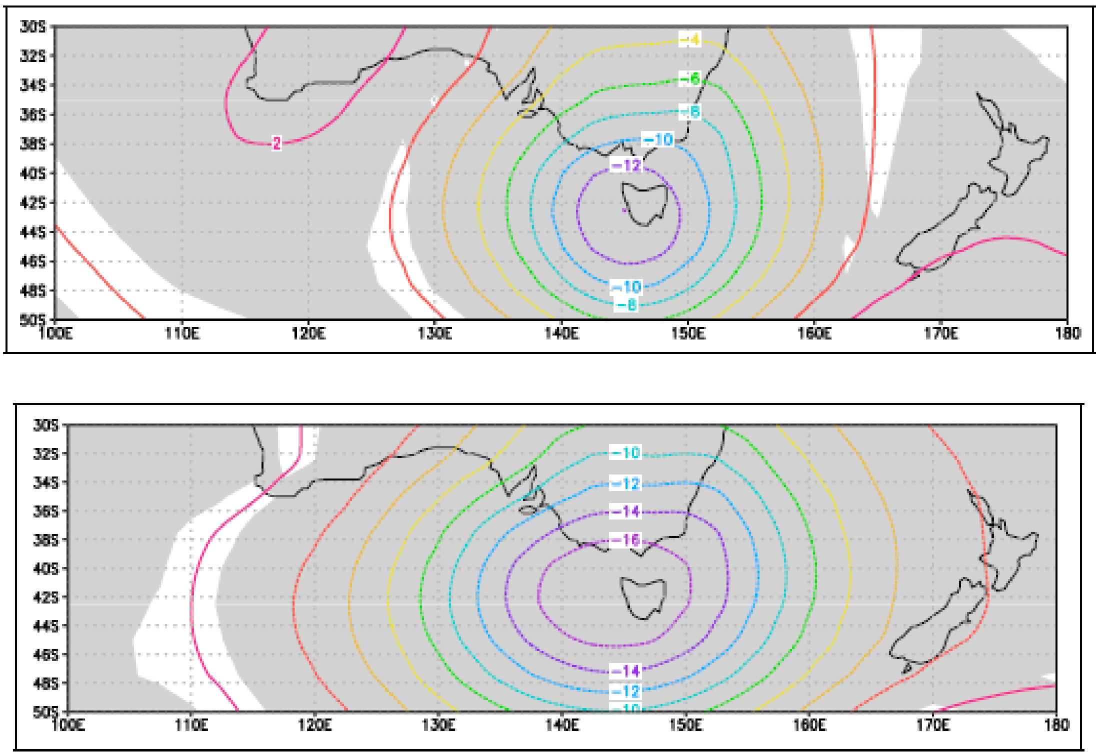

Fig. 2: Composite pressure anomaly for (a, top) all cyclone centres identified in the reanalysis in the target area and (b, bottom) all times identified by the sequence matching process.

International Arctic Buoy Program data and the diagnosis of strong surface winds over the Arctic Ocean

Ian Simmonds and Tess Parker

School of Earth Sciences
The University of Melbourne
Victoria, 3010, Australia
simmonds@unimelb.edu.au

The IABP has been deploying buoys in the Arctic since 1979, and these provide an immensely valuable resource in a region virtually devoid of conventional surface observations. We are exploring the use of 6-hourly buoy SLP data to investigate the occurrence of strong wind events in the basin. A goal is to compare the organization of extreme storminess so-derived with that obtained from regional or global reanalyses (e.g., Simmonds et al. 2008).

Figure 1(a) shows the time mean SLP recorded by a set of buoys during the month of August 2002 (the mean for each buoy is plotted at the centre of gravity of its locations during the month). Panel (b) of the Figure shows the corresponding monthly mean MSLP analysis from the ERA-40 (Uppala et al. 2005). Clearly there is strong consistency between the two presentations.

Assuming geostrophy, the surface wind vector can be deduced from a trio of buoys. This is achieved by fitting a (unique) plane through the three observations and the geostrophic velocity vector determined from the directional slope of the plane (using the techniques of, e.g., Wang et al. 2009). We are investigating performing the appropriate quality controls and choosing a number of appropriate buoy triangles from which to estimate the wind velocity, thought to be applicable at the centroid of each triangle. We exemplify this method by application to the monthly mean pressures presented above. Figure 2 presents the mean velocity vectors derived from this approach.

References

Simmonds, I., C. Burke and K. Keay, 2008: Arctic climate change as manifest in cyclone behavior. *Journal of Climate,* **21,** 5777-5796.

Uppala, S. M., P. W. Kallberg, A. J. Simmons, U. Andrae, V. D. Bechtold, M. Fiorino, J. K. Gibson, J. Haseler, A. Hernandez, G. A. Kelly, X. Li, K. Onogi, S. Saarinen, N. Sokka, R. P. Allan, E. Andersson, K. Arpe, M. A. Balmaseda, A. C. M. Beljaars, L. Van De Berg, J. Bidlot, N. Bormann, S. Caires, F. Chevallier, A. Dethof, M. Dragosavac, M. Fisher, M. Fuentes, S. Hagemann, E. Holm, B. J. Hoskins, L. Isaksen, P. Janssen, R. Jenne, A. P. McNally, J. F. Mahfouf, J. J. Morcrette, N. A. Rayner, R. W. Saunders, P. Simon, A. Sterl, K. E. Trenberth, A. Untch, D. Vasiljevic, P. Viterbo and J. Woollen, 2005: The ERA-40 re-analysis. *Quarterly Journal of the Royal Meteorological Society,* **131,** 2961-3012.

Wang, X. L., F. W. Zwiers, V. R. Swail and Y. Feng, 2009: Trends and variability of storminess in the Northeast Atlantic Region, 1874-2007. *Climate Dynamics,* doi: 10.1007/s00382-008-0504-5.

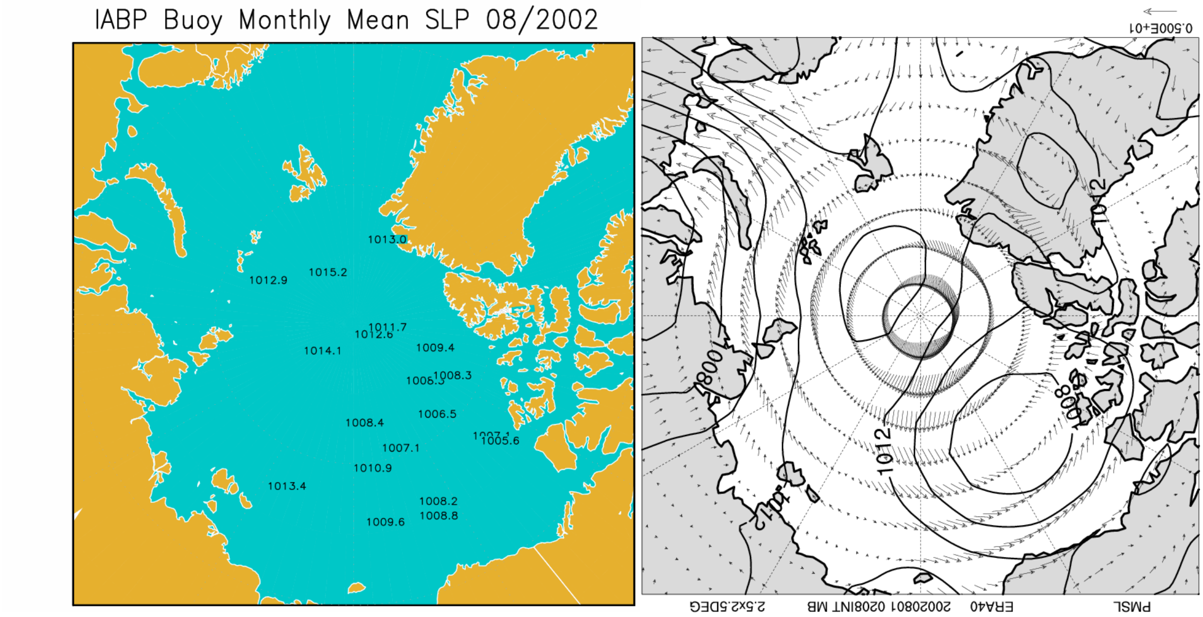

Figure 1: (a, left) Mean SLP recorded by a set of buoys during the month of August 2002 (the mean for each buoy is plotted at the centre of gravity of its locations during the month) and (b, right) the corresponding monthly mean MSLP analysis from the ERA-40.

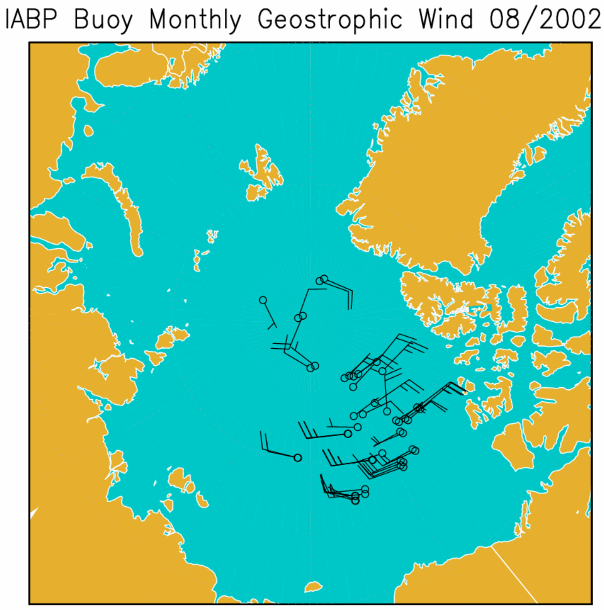

Figure 2: Geostrophic surface wind vectors deduced from a subsample of 'quality controlled' trio of buoys for the mean SLP during August 2002.

Summer Arctic basin cyclone properties in the ERA-40 data set

Ian Simmonds*, Craig Burke** and Kevin Keay*

*School of Earth Sciences
The University of Melbourne
Victoria, 3010, Australia
simmonds@unimelb.edu.au

**National Meteorological and
Oceanographic Centre
Australian Bureau of Meteorology
700 Collins Street, Docklands 3008, Australia

In the early part of the twentieth century the 'glacial anticyclone theory' of Arctic climate was generally accepted. However, these days it is known that the Arctic basin is host to a range of isobaric systems and intense cyclones year round. In this communication we present the structure of some key climatological characteristics of summer cyclonic systems in the Arctic basin.

We compile these climatologies using the ERA-40 re-analysis (Uppala et al. 2005) for summers (JJA) over the period 1958-2002. The cyclonic systems are identified and tracked with the Melbourne University cyclone tracking scheme (Simmonds and Murray 1999, Simmonds and Keay 2000a, b). The algorithm identifies both 'open and 'close' systems, and also computes a raft of characteristics for each identified cyclone, including Radius and Depth (see, e.g., Lim and Simmonds (2007) These statistics provide significantly more information than would be presented by cyclone counts alone.

The density of systems (the mean number per analysis found in a 10^3 (deg. lat.)^2 normalizing area) is presented in Fig. 1(a). A region of frequencies in excess of 3 is found in the central Arctic. There is known to be a winter centre of cyclonic activity off northwest Norway (see, e.g., Simmonds et al., 2008); in summer there is also a local maximum there but it is much more modest. It is of value to interpret this summer distribution in terms of the distribution of cyclogenesis. Fig. 1(b) shows the regions of greatest genesis to lie over the relatively warmer regions off Alaska and northern Norway.

The largest cyclones (greatest radius) are found in the central Arctic (Fig. 2(a)). The systems found in the basin are rather similar in size to those further south (Simmonds 2000) and exceed 5 deg. lat. over a significant portion of the domain. As to the net 'influence' of these summer cyclones, the greatest mean cyclone depths (in excess of 5 hPa) (Fig. 2(b)) are found in the broad region centered on the Pole.

Lim, E.-P., and I. Simmonds, 2007: Southern Hemisphere winter extratropical cyclone characteristics and vertical organization observed with the ERA-40 reanalysis data in 1979-2001. *J. Climate,* **20,** 2675-2690.

Simmonds, I., 2000: Size changes over the life of sea level cyclones in the NCEP reanalysis. *Mon. Wea. Rev.,* **128,** 4118-4125.

Simmonds, I., and R. J. Murray, 1999: Southern extratropical cyclone behavior in ECMWF analyses during the FROST Special Observing Periods. *Wea. Forecasting,* **14,** 878-891.

Simmonds, I., and K. Keay, 2000a: Mean Southern Hemisphere extratropical cyclone behavior in the 40-year NCEP-NCAR reanalysis. *J. Climate,* **13,** 873-885.

Simmonds, I., and K. Keay, 2000b: Variability of Southern Hemisphere extratropical cyclone behavior 1958-97. *J. Climate,* **13,** 550-561.

Simmonds, I., and Coauthors, 2008: Arctic climate change as manifest in cyclone behavior. *J. Climate,* **21,** 5777-5796.

Uppala, S. M., and Coauthors, 2005: The ERA-40 re-analysis. *Quart. J. Roy. Meteor. Soc.,* **131,** 2961-3012.

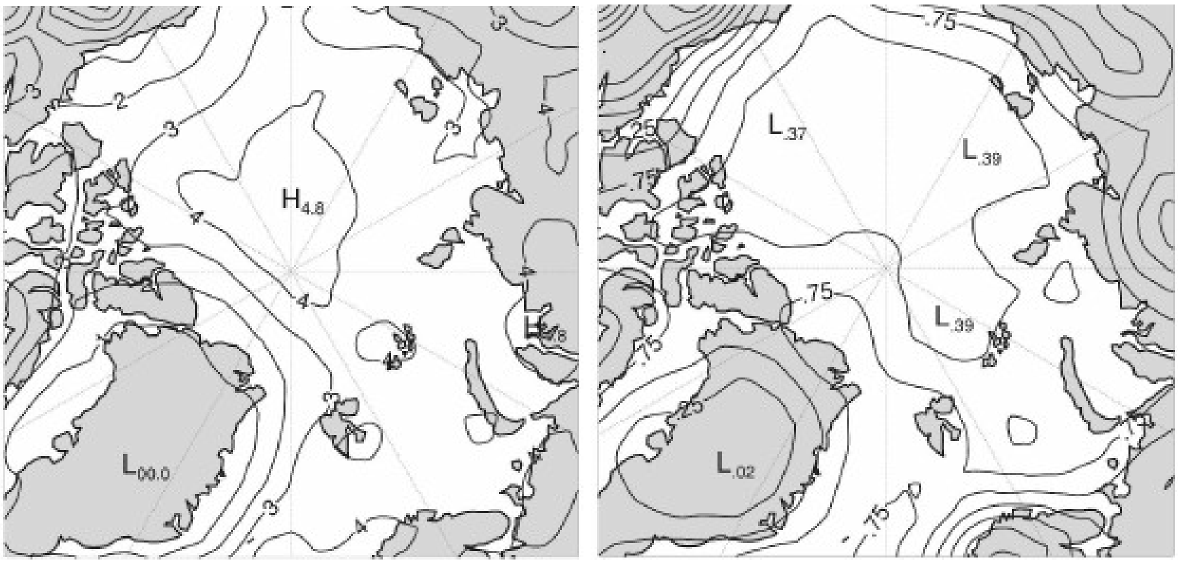

Figure 1: (a, left) System density (the mean number of cyclones found in a 10^3 (°lat)^2 area per analysis) and (b, right) density of the rate of cyclogenesis (systems formed in a 10^3 (°lat)^2 area per day. Both plots are for the summer season.

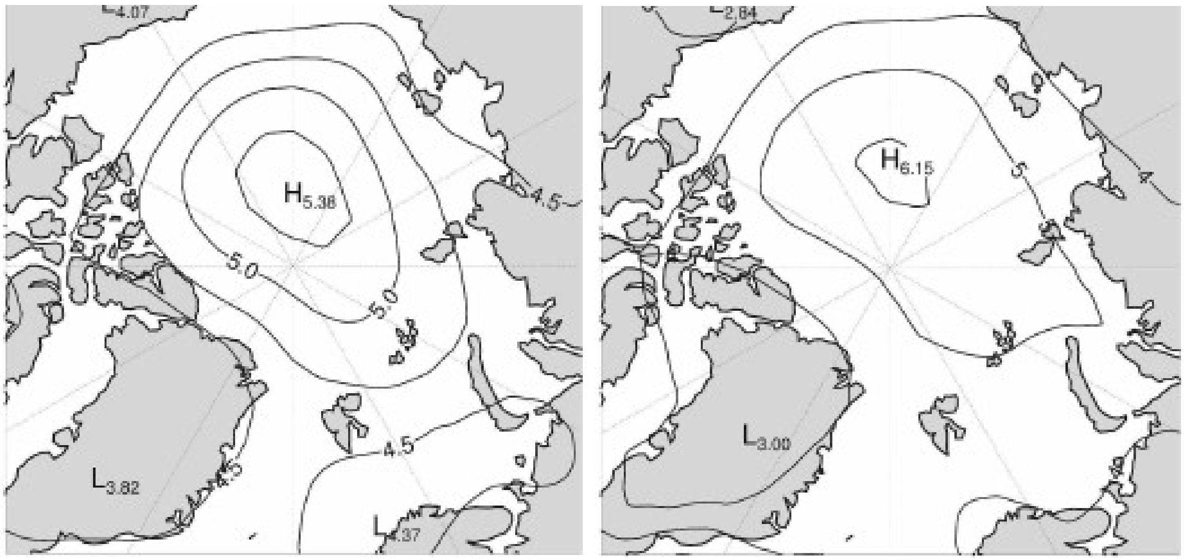

Figure 2: Mean summer distribution of the (a, left) Radius and (b, right) Depth of cyclones. The units are °lat and hPa, respectively.